
This is an electronic reprint of the original article.
This reprint may differ from the original in pagination and typographic detail.

Viitala, Hanna; Taskinen, Pekka; Lindberg, Daniel

Experimental determination and thermodynamic optimization of the CuCl–ZnCl₂, ZnCl₂–FeCl₃, CuCl–FeCl₃, CuCl–CuCl₂, FeCl₂–FeCl₃, FeCl₂–CuCl₂ and CuCl–PbCl₂ phase equilibria

Published in:

Calphad: Computer Coupling of Phase Diagrams and Thermochemistry

DOI:

[10.1016/j.calphad.2019.101667](https://doi.org/10.1016/j.calphad.2019.101667)

Published: 01/12/2019

Document Version

Peer-reviewed accepted author manuscript, also known as Final accepted manuscript or Post-print

Published under the following license:

CC BY-NC-ND

Please cite the original version:

Viitala, H., Taskinen, P., & Lindberg, D. (2019). Experimental determination and thermodynamic optimization of the CuCl–ZnCl₂, ZnCl₂–FeCl₃, CuCl–FeCl₃, CuCl–CuCl₂, FeCl₂–FeCl₃, FeCl₂–CuCl₂ and CuCl–PbCl₂ phase equilibria. *Calphad: Computer Coupling of Phase Diagrams and Thermochemistry*, 67, Article 101667. <https://doi.org/10.1016/j.calphad.2019.101667>

This material is protected by copyright and other intellectual property rights, and duplication or sale of all or part of any of the repository collections is not permitted, except that material may be duplicated by you for your research use or educational purposes in electronic or print form. You must obtain permission for any other use. Electronic or print copies may not be offered, whether for sale or otherwise to anyone who is not an authorised user.

Experimental determination and thermodynamic optimization of the CuCl-ZnCl₂, ZnCl₂-FeCl₃, CuCl-FeCl₃, CuCl-CuCl₂, FeCl₂-FeCl₃, FeCl₂-CuCl₂ and CuCl-PbCl₂ phase equilibria.

Hanna Viitala^{1,*}, Pekka Taskinen^{1,*}, Daniel Lindberg¹

¹Aalto University School of Chemical Technology, Department of Chemical Engineering and Metallurgy, P.O. Box 16100, FI-00076 Aalto, Espoo (Finland)

¹Metallurgical Thermodynamics and Modelling, Kemistintie 1, 02150 Espoo, Finland

E mail*: hanna.sahivirta@aalto.fi

E mail: pekka.taskinen@aalto.fi

E mail: daniel.k.lindberg@aalto.fi

Abstract

In copper flash smelting, flue dust causes corrosion problems in the heat recovery boiler of the gas train due to formation of dust accretions on the boiler walls. Within these, presence of heavy metal chlorides results in formation of molten salt deposits causing rapid corrosion. CuCl-ZnCl₂, FeCl₃-ZnCl₂ and CuCl-FeCl₃ systems were studied experimentally by equilibration-quenching, scanning electron microscopy and energy-dispersive X-ray spectroscopy in order to evaluate melting behaviour of these chlorides, typically present in the corrosive dust deposits. In addition, CuCl-PbCl₂, CuCl-CuCl₂, FeCl₂-FeCl₃ and CuCl₂-FeCl₂ phase diagrams were optimized incorporating and evaluating all available phase diagram and thermodynamic data on the systems. The modified quasi-chemical model was used to describe the thermodynamic properties of molten phases and compound energy formalism was used to model the terminal solid solutions. The calculated phase diagrams are presented and compared with experimental observations as well as with all available phase diagram data from existing literature.

Key words: Thermodynamic modelling, Chloride solutions, Equilibration-Quenching method, Phase diagram

1. Introduction

In the copper flash smelting, flue dust can cause severe problems in the gas train, used e.g. for separating dust from the SO₂-rich process off gas, by forming corrosive accretions on walls of the heat recovery boiler. These dust build-ups in the boiler need to be cleaned regularly and potential corrosion damage checked. This requires a shut-down of the flash smelting process. Copper and zinc among other elements having high vapour pressures vaporize during smelting of the sulfidic copper concentrations forming dust when the process gas, containing close to 50 vol% SO₂, cools down. Also, particles of solid or liquid oxides originating from the ore get transported with process gas to the heat recovery boiler as a mechanical entrainment. [1]

The dust build-ups on the boiler walls are formed partly by direct impact of particles and partly by vapour condensation. The initial deposition takes place by the condensation of vapours that contain zinc, lead, arsenic and other metals having high vapour pressures. Also low melting point eutectics of alkali salts such as chlorides and sulphates can act as sticky cohesive particles attaching to the boiler walls. The fine particles landing on the surface of the porous dust deposit react in the SO₂-rich atmosphere at boiler wall temperatures to sulphates. The process gas within the boiler contains SO₂, O₂, SO₃, H₂O and N₂ gases that

diffuse into the porous accretions to form a stagnant gas layer within the dust deposit. The composition of this gas layer may differ greatly from the composition of the process gas flow on the surface of the accretion. Locally HCl and H₂SO₄ are formed and even reducing atmosphere may exist within the dust deposit, allowing new reactions to take place. The local micro-atmosphere may enable metal sulphates to be reduced to secondary sulphides and even metallic components. Within the dust accretion layer, compounds may form that would not be stable in the bulk atmosphere of the boiler. [1] This may be the mechanism by which e.g. chlorides of Cu, Fe, Pb and Zn are formed within the deposit.

Our previous research [2,3] showed the corrosion damage of the boiler to be primarily a result of formation of molten salt mixtures within the dust deposit leading to rapid pitting corrosion. The presence of heavy metal chlorides reduce the melting points of the dust deposit enough so that molten salts can exist at the operating temperatures (250 °C - 350 °C) of the boiler wall. The purpose of this research is to study the melting behaviour of CuCl, CuCl₂, ZnCl₂, PbCl₂, FeCl₂ and FeCl₃-systems because these chlorides are typically found in the copper smelter flue dust deposits [2,3].

2. Literature data

Only limited amount of research concerning phase equilibrium diagrams of CuCl-CuCl₂-FeCl₂-FeCl₃-ZnCl₂-PbCl₂ system exist in literature. However, understanding the reactions of this system and especially the melting conditions is of great importance in order to understand the circumstances governing the corrosion processes in the heat recovery boiler of a copper flash smelter. Normally, no single technique of studying phase equilibria may be completely satisfactory since all the experimental methods are subjected to sources of error typical to each method. Rather the final evaluation of phase equilibria based on information derived from several techniques may help to evaluate the phase equilibria relations more accurately. [4]

The ZnCl₂-CuCl, ZnCl₂-FeCl₃ and CuCl-FeCl₃ phase diagrams have been measured previously over hundred years ago using thermal analysis. In this research, the data of the previous research is supplemented with experimental part involving the equilibration and quenching method as well as with thermodynamic modelling part. Chloride systems have not been studied previously using the equilibration and quenching technique, which provides some improvements to the heating and cooling curves. For example, compositional changes during the equilibration have less effect on the final results, since the phase compositions are measured after the experiment rather than before it. In addition, problems such as vaporization effects can be detected by scanning electron microscopy. [5, 6] The obtained phase equilibria are important experimental data for the optimization of thermodynamic parameters, which in turn can be utilized for calculation of phase diagrams.

2.1 The CuCl-ZnCl₂ system

The CuCl-ZnCl₂ binary phase diagram was measured previously by Herrmann et al. [7] using thermal analysis. Herrmann et al. [7] determined the eutectic point of the system to occur at composition of 90 weight% of ZnCl₂ at 243 °C. Later Palkin et al. [8] repeated the measurement of the liquidus curve using the same method. They found the eutectic point at the composition of 91 weight% of ZnCl₂ at 283 °C. They did not attempt to measure solid solubilities of the terminal phases.

Herrmann et al. [7] measured the melting point of pure CuCl to be 424 °C and pure ZnCl₂ to be 261,5 °C. The obtained melting point is very different from the value of 318 °C reported and assessed by Robelin et al. [9]. This type of error may be related to the problem of very rapid water intake of zinc chloride during its weighing and handling, and the tendency of zinc chloride to require undercooling to crystallize. Difficulties in the handling of zinc chloride due to its rapid water absorption from the air were also reported

by Hermann et al. Palkin et al. [8] did not mention whether the melting points of CuCl and ZnCl₂ were measured in their study, but reported 434 °C for CuCl and 319 °C for ZnCl₂. These values are closer to the currently accepted melting points of CuCl and ZnCl₂ [10].

ZnCl₂ and CuCl were also reported to have solid solubilities with each other. CuCl with a higher melting point dissolves maximum 18 wt% ZnCl₂ and CuCl was measured to dissolve maximum 5wt% ZnCl₂. The solubility curves of ZnCl₂ in solid CuCl and CuCl in solid ZnCl₂ could not be measured all the way along the solidus because they were no longer thermally nor microscopically measurable. Zinc chloride rich side of the phase diagram starting from the eutectic point towards pure ZnCl₂ requires 4 °C of undercooling to crystallize. Otherwise, the system crystallizes without undercooling. [7]

Mayer et al. [11] have conducted vapour pressure measurements of different CuCl-ZnCl₂ mixtures determining partial pressure of ZnCl₂ in equilibrium conditions using a Bourdon-Manometer.

2.2 The ZnCl₂-FeCl₃ system

Herrmann et al. measured phase diagram of the FeCl₃-ZnCl₂ system, which is similar to the CuCl-ZnCl₂ system by heating and cooling curves. Chloride salts rarely form mixed crystals with each other but FeCl₃-ZnCl₂ exhibits that feature. The system also has one miscibility gap in the solid region of the diagram. FeCl₃ was measured to dissolve less than 13 wt% of ZnCl₂ and the maximum solubility of FeCl₃ in ZnCl₂ was measured between 5 and 10 wt%. [7]

The authors had difficulties of measuring the eutectic temperature with good repeatability. The average of the measurements was used and the eutectic temperature was reported to be 214 °C. The eutectic point was reported to be situated at 70 wt% of ZnCl₂ in the FeCl₃-ZnCl₂-phase diagram. Pure FeCl₃ crystallizes without undercooling, but between the compositions 18 – 70 wt% of ZnCl₂, the system requires 1 to 10 °C of undercooling to crystallize. The melting point of FeCl₃ was reported to be 298 °C. [7].

2.3 The CuCl-FeCl₃, CuCl-CuCl₂, FeCl₂-FeCl₃ and CuCl₂-FeCl₂ systems

The CuCl-FeCl₃ system has been reported by Hermann et al. [7] and TeCl₄-CuCl-FeCl₃ system was measured by Kozachenko et al. [12] using differential thermal analysis. However, the binary CuCl-FeCl₃, used by Kozachenko et al. [12] was taken from Herrmann et al [7]. Herrmann et al [7] observed formation of a congruently melting double salt Cu₂Cl₂(FeCl₃)₂ at composition of 62 wt % of FeCl₃ at 320 °C. CuCl and FeCl₃ have not been reported to have solid solubility in each other. Hermann et al. have measured the eutectic points of the system at composition of 50 wt % of FeCl₃ at 304 °C and at 88 wt % of FeCl₃ at 263 °C. No region in the CuCl-FeCl₃ diagram requires undercooling to crystallize [7].

CuCl-CuCl₂ phase diagram has been measured by Biltz et al. [13] and by Safonov et al. [14] using thermal analysis. The phase diagrams are compatible with each other both having eutectic temperature at 378 °C and at 13 mol% of CuCl₂. Optimizing the behaviour of the CuCl-CuCl₂, FeCl₂-FeCl₃ and CuCl₂-FeCl₂ systems was used for the optimization the CuCl-FeCl₃ phase diagram, since some CuCl₂ and FeCl₂ crystals are expected to be present in the system as well. The melting point of pure CuCl₂ was not observed as it decomposed at 614 °C. Based on extrapolations from the experimental liquidus points, the melting temperature of CuCl₂ was estimated to be (630±10)°C. [13]

FeCl₂-FeCl₃ phase diagram has been measured by Schäfer et al. [15] using thermal analysis, visual observations and isothermal distillation. . It was observed to be a simple eutectic system with eutectic point at 298 °C, with 13.5 mol% of FeCl₂.

The phase equilibrium of the $\text{CuCl}_2\text{-FeCl}_2$ system was studied by Korzhukov et al. [16] with thermal analysis using samples in sealed quartz ampoules. The phase equilibria showed a eutectic type behaviour of the system. The melting point of CuCl_2 was measured to be $596\text{ }^\circ\text{C}$ during heating. A solid phase transition of CuCl_2 was observed at $488\text{ }^\circ\text{C}$. In our present optimization, this transition was not included due to the lack of confirming data for the solid phase transition.

2.4 CuCl-PbCl_2

Herrmann et al. [7] measured the phase diagram of CuCl-PbCl_2 using thermal analysis, and Coleman et al. [17] measured the phase equilibria using hot stage microscopy. The system is a simple eutectic system with eutectic point at $281.4\text{ }^\circ\text{C}$ at 34 weight% of CuCl according to measurements of Herrmann et al. [7] and Coleman et al. [17] measured the eutectic point at $280\text{--}284\text{ }^\circ\text{C}$ at 30 wt% of CuCl .

Herrmann et al. [7] observed undercooling between $3\text{ }^\circ\text{C}$ - $7\text{ }^\circ\text{C}$ at compositions between 30 – 40 wt% of CuCl . They had difficulties in measuring the eutectic temperature and an average of the measurements was reported as the eutectic temperature.

3. Experimental procedure

The phase boundary compositions of the binary CuCl-ZnCl_2 , CuCl-FeCl_3 and $\text{FeCl}_3\text{-ZnCl}_2$ systems were measured by an equilibration and quenching method, which involved equilibration in isothermal conditions, a rapid quenching, and direct measurement of equilibrium phase compositions with scanning electron microscopy. [5, 6] The thermodynamic constraints of measuring the phase diagrams are based on the Gibbs phase rule (1).

$$f = c - p + 2 \quad (1)$$

where the variable f is called the degree of freedom. c is the number of components of the system and p is the number of phases. The binary systems were measured at constant pressure 1 atm, thus the constant 2, representing alterable intensive variables such as temperature and pressure, is reduced to one. When the number of components (CuCl , ZnCl_2 and FeCl_3) is two in the binary systems, the phase rule shows that within a single phase region of the phase diagram, there are two degrees of freedom. Then, temperature and composition may be varied independently and in a two-phase region, temperature may be varied, but at any temperature the compositions of the coexisting two phases are fixed. [18]

$$f = c - p + 1 = 3 - p \quad (2)$$

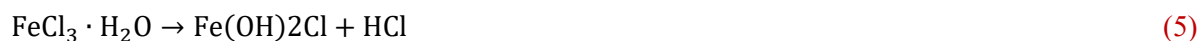
The experiments were conducted at isothermal conditions reducing the f by one and resulting in a fully defined system ($f=0$), which means that changing the system composition changes only the relative amounts of the two phases, but the phase compositions of the two coexisting phases remain unchanged. The compositions of all phases in equilibrium can be determined, such as the compositions of solid phases coexisting with the liquid. [18]

Anhydrous powders of CuCl , ZnCl_2 and FeCl_3 were used as starting materials. The samples were prepared by weighing the chloride powders before each experiment with a calibrated Mettler Toledo AB204-S semi-microbalance, that has a measurement accuracy of $\pm 0.1\text{ mg}$, and mixing them according to predetermined starting compositions. The starting compositions were selected so that two phases could be obtained during equilibration. The sample size was small (0.4 g) in order to enhance the achievement of equilibrium and reaching higher quenching rates. List of chemicals used and their purities are shown in table 1.

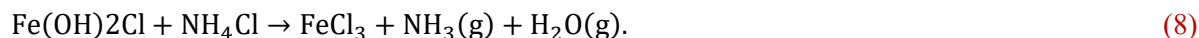
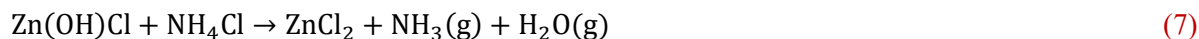
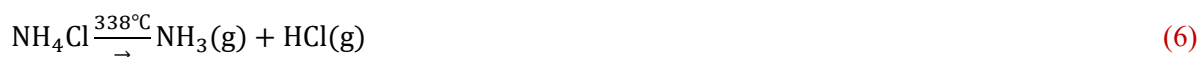
Table 1. Starting materials used during the equilibration experiments.

Material	Manufacturer	Purity
Zinc chloride ZnCl ₂	SIGMA ALDRICH	Reagent grade ≥ 98 %
Cuprous Chloride CuCl	SIGMA ALDRICH	Reagent grade ≥ 97 %
Ferric Chloride FeCl ₃	SIGMA ALDRICH	Reagent grade ≥ 97 %
Ammonium Chloride NH ₄ Cl	SIGMA ALDRICH	99,99 %
Argon Ar	AGA	99,99 %

Some difficulties occurred that must be taken into consideration during the equilibration when dealing with ZnCl₂ and FeCl₃. Despite the fact that anhydrous chlorides were used as starting materials, the anhydrous form of ZnCl₂ is highly hygroscopic, absorbing moisture rapidly from the ambient air and turning into one of five hydrates [19, 20]. It is difficult to work with anhydrous ZnCl₂ fast enough in ambient air in order to avoid hydration and if the hydrated zinc chloride is attempted to be dried by evaporating the crystalline water, oxychloride is first formed according to reactions (3) – (4). [21] FeCl₃ is highly hygroscopic as well and on exposure to air forms a series of hydrates with 2, 5 and 6 water molecules [22]. Also, when hydrated FeCl₃ is dried by heating oxychloride is formed instead of anhydrous FeCl₃ according to reaction (5). CuCl on the other hand is fairly stable in exposure to air [23].



The sample mixtures were equilibrated in pyrex glass crucibles. In order to dry the hygroscopic chlorides, ammonium chloride was added in the bottom of the crucibles. The sample mixtures were added on top of the ammonium chloride layer so that HCl and NH₃ gases rinse the chloride powders according to reactions (6) – (8). The crucibles were covered by a lid that does not completely seal the crucible, but rather slows the rate of gas exchange with the environment, so that water vapour and NH₃ gases can exit the system.



In order for ammonium chloride to dry the samples, they were first kept at 340 °C for half an hour after which temperature was dropped to the equilibration temperature. Most chlorides are difficult to melt because they have high vapour pressures and they volatilize at relatively low temperatures, except for the alkali and alkaline earth chlorides. For this reason, the samples were not premelted above the liquidus line.

The samples were equilibrated in a vertical electrical resistance tube furnace (Lenton CSC12/-/450V, controller by Eurotherm 3216CC) at isothermal conditions. The samples were suspended on a wire within a fused quartz work tube in the hot zone of the furnace. The location of the hot section within the work tube was located by measuring a temperature profile of the furnace. A calibrated PT100 resistance sensor, connected to Keithley 2010 DMM multimeter (Cleveland, OH, USA), having measurement accuracy of

$\pm 0,1$ °C, was placed next to the sample for recording the sample temperature. The temperature of the hot section was measured and logged every five seconds during equilibration with an NI LabVIEW temperature logging program. The temperature profile of the furnace was measured by moving the calibrated resistance sensor from the cold section on top of the furnace downwards to the cold section in the bottom of the furnace in one cm intervals and measuring the temperature of the furnace at each point. The hot zone of the furnace, where temperature variations were within ± 1 °C, was measured to be 8 cm long at 300 °C in the middle of the furnace. The studied samples were small (approximately 0.5 cm long) and thus according to the temperature profile measurement, the uncertainty of the sample temperature was estimated to be no more than ± 1 °C next to the resistance sensor placed in the middle of the hot section during the experiments. Argon was led to the furnace through a rotameter and the furnace was flushed with argon before lifting the sample to the target temperature in order to avoid oxidation. The sample was pulled to the hot section of the furnace from the bottom by pulling it on a wire from the top of the furnace. A schematic diagram of the furnace setup used for the equilibration is presented in figure 1.

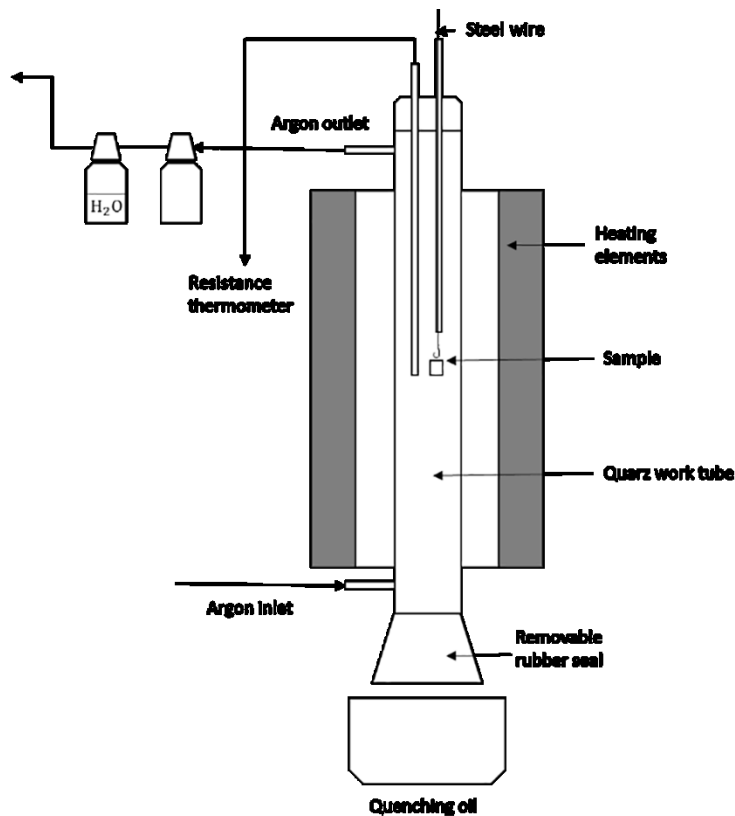


Figure 1. Schematic diagram of the furnace setup used for equilibration annealing at isothermal, isobaric experimental conditions, and for quenching.

Whether equilibrium is achieved during the annealing, affects the accuracy and reliability of the results. Equilibrium conditions were confirmed by conducting equilibration experiments at the same temperature with the same sample materials but with different equilibration times. This was done to confirm homogeneity of the phases and that no further changes occur in the sample composition as the equilibration time increases. The experimental conditions are shown in table 2. After a sufficient time of equilibration, the samples were quenched in cooled mineral oil (Shell Ondina) due to their highly hygroscopic nature and mounted in epoxy. The sample preparation process for the SEM-EDS analysis was water free in order to avoid contamination of the samples with moisture. The samples were polished with SiC papers P80, P240,

P400, P800, P2000 and P4000 in the same order, using mineral oil as lubricant to expose a suitable cross section for SEM-EDS analysis. After polishing, the oil was removed by washing in petroleum ether in an ultrasonic bath, after which they were coated with carbon (Leica EM SCD050 Coater, Leica Microsysteme, GmbH, Vienna).

Table 2. The experimental equilibration temperatures, starting compositions and times sufficient to reach equilibrium for the systems CuCl-ZnCl₂, FeCl₃-ZnCl₂ and CuCl-FeCl₃.

T/°C	Equilibration composition in wt%	Sufficient equilibration time /h
CuCl-ZnCl₂		
230	70 CuCl 30 ZnCl ₂	20
240	70 CuCl 30 ZnCl ₂	20
250	70 CuCl 30 ZnCl ₂	20
300	75 CuCl 25 ZnCl ₂	6
350	75 CuCl 25 ZnCl ₂	6
FeCl₃-ZnCl₂		
190	80 FeCl ₃ 20 ZnCl ₂	20
214	80 FeCl ₃ 20 ZnCl ₂	20
230	80 FeCl ₃ 20 ZnCl ₂	20
214	10 FeCl ₃ 90 ZnCl ₂	20
230	10 FeCl ₃ 90 ZnCl ₂	20
250	80 FeCl ₃ 20 ZnCl ₂	6
CuCl-FeCl₃		
307	90 CuCl 10 FeCl ₃	6
307	55 CuCl 45 FeCl ₃	6
350	90 CuCl 10 FeCl ₃	4

The samples were analyzed with a scanning electron microscope (LEO 1450, Carl Zeiss Microscopy, Germany) including a X-Max type EDS (Energy dispersive spectrometer) detector by Oxford Instruments (Abingdon, UK). The results of the element analysis of the phases obtained during equilibration were measured with INCA Energy software by Oxford instruments. Mineral standards by Astimex Scientific (Toronto, Canada) were used in the EDS-analysis. Fe was calibrated with hematite (Fe₂O₃), Cu was calibrated with cuprite (Cu₂O), Zn was calibrated with sphalerite (ZnS) and chlorine was calibrated with tugtupite (Na₄AlBeSi₄O₁₂Cl). INCA Energy software has a XPP-type matrix correction algorithm based on a Phi-Rho-Z approach [24]. Due to the porosity of the samples, the EDS-results were normalized for better comparability.

4. Thermodynamic modelling

The CuCl-ZnCl₂, FeCl₃-ZnCl₂, CuCl-FeCl₃, CuCl₂-CuCl, FeCl₂-FeCl₃, CuCl₂-FeCl₂ and CuCl-PbCl₂ phase diagrams were optimized using FactSage 7.2 thermochemical software, which calculates phase equilibria based on minimization of the Gibbs energy [10]. Molar Gibbs energy of a solution consists of three parts according the equation (9) [25, 26].

$$G_m = G_{mix}^{\circ} + \Delta G_{mix}^{ideal} + \Delta G_{mix}^{Excess} \quad (9)$$

in which G_{mix}° represents Gibbs energy of pure components of the system, ΔG_{mix}^{ideal} is the ideal mixing term and G_{mix}^{Excess} is the excess Gibbs energy of mixing. [25, 26, 27]

4.1 Thermodynamic data for pure compounds

The thermodynamic data ($\Delta H_{298.15K}^\circ$, $S_{298.15K}^\circ$ and C_p) for the stoichiometric components used for modelling the solid and liquid phases are given in table 3. The thermodynamic data were taken from FactPS (pure substance database) version 7.2 [10].

Table 3. Thermodynamic properties of stoichiometric phases used in the optimizations of this study. S, L and G refer to solid, liquid and gas phases.

		T Range (K)	$\Delta H_{298.15K}^\circ$ (J/mol)	$S_{298.15K}^\circ$ (J/mol*K)	C_p (J/mol*K)
ZnCl₂	S	298.15 to 591	-415649	106.5991	62.941+ 0.028665(T/K)
	L	298.15 to 1005	-396210.7183	139.3450	65.835+0.023129(T/K)
	G	298.15 to 2000	-265684	276.5625	62.32014-481616.8(T/K) ⁻²
CuCl₂	S	298.15 to 1500	-205853	108.085	82.501348+0.0033626(T/K)- 3891.802686(T/K) ⁻² - 3462.1776787(T/K) ⁻¹
CuCl	S	298.15 to 703	-138072	87.027	27.254489+0.02527(T/K)- 4350452.10488(T/K) ⁻² - +18685.98889 (T/K) ⁻¹
	S	703 to 1500			63.12945+0.0031(T/K)- 1249594.42050(T/K) ⁻²
	L	298.15 to 3000	-131163.515887	93.7907432	66.944
	G	298.15 to 6000	91086	237.097556	37.504397+0.000456(T/K)- 161925.941004(T/K) ⁻² - 171.74490(T/K) ⁻¹
FeCl₃	S	298.15 to 577	-399405	142.336	3436.4600-1.25996(T/K)+ 674287.32793(T/K) ⁻¹ - 90229.71490(T/K) ^{-1/2}
	L	298.15 to 1500	-362717.83951	200.67447	133.888
	G	298.15 to 6000	-253132	344.09655	83.146989-564712.44410(T/K) ⁻² - +23900758.97238(T/K) ⁻³
FeCl₂	S	298.15 to 950	-341833	117.947	82.80332+0.0068044(T/K)- 107284.55334(T/K) ⁻² - 2075.22264(T/K) ⁻¹
	L	298.15 to 2000	-311330.874270	139.89150	102.173
	G	298.15 to 700	-141001	299.173556	63.68195-0.00033(T/K)- 181924.49566(T/K) ⁻² - 1183.141998(T/K) ⁻¹
	G	700 to 2800			195.198277-0.00953(T/K)- 17160773.4723696(T/K) ⁻² - +149068.43684(T/K) ⁻¹ - 8071.4241448(T/K) ^{-1/2}
PbCl₂	S	298.15 to 1500	-359406	135.98	68.4910348+0.02895867(T/K)
	L	298.15 to 500	-344257.0628435	153.389681	68.3906557+0.02920894(T/K)
	L	500 to 2000			111.504
	G	298.15 to 1200	-174054	317.095556	58.676766-0.00019371896(T/K)- -190462.9674556(T/K) ⁻² - 385.81862084387(T/K) ⁻¹
Cl₂	G	298.15 to 1600		222.9695629	20.6807665+316713.29295(T/K)- ² +0.191057669(T/K) ^{1/2} - +591.2612196(T/K) ^{-1/2} - 8299.370359(T/K) ⁻¹

4.2 Liquid solutions of **CuCl-ZnCl₂**, **ZnCl₂-FeCl₃**, **CuCl-FeCl₃**, **CuCl-CuCl₂**, **FeCl₂-FeCl₃**, **FeCl₂-CuCl₂** and **CuCl-PbCl₂** systems

The liquid solutions of the chloride systems of this study were modelled according to the modified quasi-chemical model, based on the assumption of random mixing of nearest neighbour pairs. The extent of short-range ordering of the solution is determined by calculating the equilibrium amount of the second-nearest-neighbour (cation-cation) pairs formed according to reaction (10). [28-33] In the case of studied systems the anion sublattice only contains chloride, which is why the model only considers formations and mixing of cation-cation pairs on the cation sublattice [34].

$$(A - Cl - A)_{\text{pair}} + (B - Cl - B)_{\text{pair}} = 2(A - Cl - B)_{\text{pair}} \Delta g_{AB/Cl} \quad (10)$$

in which $\Delta g_{AB/Cl}$ is a modelling parameter representing the non-configurational Gibbs energy change of the cation-cation pair formation. [28-31] If the Gibbs energy change of the bond formation between two unlike atoms is more negative than the bonding energy between two atoms of the same kind, the system has a tendency of forming compounds and becoming more ordered. If the bonding energy between two unlike atoms is more positive compared to the energy between two same atoms, the system has a tendency to form a miscibility gap. [26, 31, 32] The total Gibbs energy of a solution is given by equation (11). [28-31]

$$G = (n_A G_A^\circ + n_B G_B^\circ) - T \Delta S^{Ideal} + \frac{n_{AB}}{2} \Delta g_{AB} \quad (11)$$

where n_{AB} is the number of pairs between cations A and B, $n_A G_A^\circ$ and $n_B G_B^\circ$ are the molar Gibbs energies of the pure components and ΔS^{Ideal} is the configurational entropy of mixing given by randomly distributing the (A-A), (B-B), and (A-B) pairs. It is expressed by equation (12).

$$\Delta S^{Ideal} = -R(n_A \ln X_A + n_B \ln X_B) - R \left[n_{AA} \ln \frac{X_{AA}}{Y_A^2} + n_{BB} \ln \frac{X_{BB}}{Y_B^2} + n_{AB} \ln \frac{X_{AB}}{2Y_A Y_B} \right] \quad (12)$$

where, n_{AA} , n_{BB} and n_{AB} are the total number of pairs in the solution. $\Delta g_{AB/Cl}$ of equations (10) and (11) is determined by equation (13). [28-31]

$$\Delta g_{AB/Cl} = \Delta g_{AB}^0 + \sum_{i \geq 1} g_{AB}^{i0} Y_A^i + \sum_{j \geq 1} g_{AB}^{0j} Y_B^j \quad (13)$$

in which g_{AB}^0 , g_{AB}^{i0} and g_{AB}^{0j} are the model parameters expressed in a polynomial form (a+bT) so that a and b are optimized from the experimental data. [28-31] Y_A^i and Y_B^j , expressed by equations (14) - (15), are coordination equivalent site fractions.

$$Y_A = Z_A Y_A / (Z_A X_A + Z_B X_B) \quad (14)$$

$$Y_B = Z_B Y_B / (Z_A X_A + Z_B X_B) \quad (15)$$

where Z_A and Z_B are coordination numbers of cations A and B and X_A and X_B are the site fractions of the sublattice. Z_A and Z_B are model parameters and they are not necessarily the real coordination numbers for the cations. [28-34] For the (A,B/Cl)-systems CuCl, ZnCl₂, FeCl₃, FeCl₂, CuCl₂ and PbCl₂ the coordination numbers Z_A and Z_B were chosen according to the relations (16) - (21).

$$Z_{Cu}^{CuCl} = 6, Z_{Cl}^{CuCl} = 6 \quad (16)$$

$$Z_{Zn}^{ZnCl_2} = 6, Z_{Cl}^{ZnCl_2} = 3 \quad (17)$$

$$Z_{Fe}^{FeCl_3} = 6, Z_{Cl}^{FeCl_3} = 2 \quad (18)$$

$$Z_{\text{Fe}}^{\text{FeCl}_2} = 6, Z_{\text{Cl}}^{\text{FeCl}_2} = 3 \quad (19)$$

$$Z_{\text{Cu}}^{\text{CuCl}_2} = 6, Z_{\text{Cl}}^{\text{CuCl}_2} = 3 \quad (20)$$

$$Z_{\text{Pb}}^{\text{PbCl}_2} = 6, Z_{\text{Cl}}^{\text{PbCl}_2} = 3 \quad (21)$$

The ratio between the second nearest neighbours Z_i and the first nearest neighbours z_i for component i , was assumed to be constant. This ratio ζ was described by equation (22) and was given a value 2.4.

$$\frac{z_i}{z_i} = \frac{\zeta}{2} \quad (22)$$

FeCl_3 crystals contain some dissolved FeCl_2 and CuCl crystals contain some CuCl_2 . For this reason, FeCl_3 - FeCl_2 , FeCl_2 - CuCl_2 and CuCl - CuCl_2 -systems were optimized based on phase diagram data by Schäfer et al. [15], Korzhukov et al. [16] and by Biltz et al. [13] and Safonov et al. [14] according to equations (23) - (25). Equation (25) describes excess melting interaction parameter for the FeCl_3 - FeCl_2 system and equation (24) describes the excess melting interaction parameter for the FeCl_2 - CuCl_2 -system. According to Ruthven et al. [35] the liquid CuCl - CuCl_2 system behaves approximately as an ideal solution due to mixing of Cu^+ and Cu^{2+} within the cation lattice. Thus, the interaction parameters for the CuCl - CuCl_2 -system were not included in the optimization. The Gibbs energy for the liquid CuCl_2 in the CuCl - CuCl_2 -system was optimized according to equation (25) because thermodynamic data for liquid CuCl_2 is not available in the Factsage databases.

$$\Delta g_{\text{Fe}(3+)\text{Fe}(2+)/\text{Cl}} = a + bT \quad (23)$$

$$\Delta g_{\text{Fe}(3+)\text{Cu}(+)/\text{Cl}} = a + bT \quad (24)$$

$$G_{\text{CuCl}_2}^{\circ(\text{Liquid})} = G_{\text{CuCl}_2}^{\circ(\text{Solid})} + (a + bT) \quad (25)$$

where a is $\Delta H_{298.15 \text{ K}}^{\circ}$ (enthalpy of liquid CuCl_2 in its reference state) and b is $S_{298.15 \text{ K}}^{\circ}$ (entropy of liquid CuCl_2 in its reference state).

4.3 Solid solutions of CuCl - ZnCl_2 and FeCl_3 - ZnCl_2 systems

CuCl - ZnCl_2 and FeCl_3 - ZnCl_2 systems contain solid solutions that were modelled according to compound energy formalism [36], in which every compound and end-member has its independent Gibbs energy of formation. Sublattice configurations for species A-D used in the modelling of this work, were constructed according to the following structures (26) - (27).

$$(\text{A}, \text{B})_{\text{m}}^{\text{S1}} (\text{C}, \text{D})_{\text{n}}^{\text{S2}} \quad (26)$$

$$(\text{A}, \text{B}, \text{C})_{\text{m}}^{\text{S1}} (\text{D})_{\text{n}}^{\text{S2}} \quad (27)$$

where the subscripts m and n give the ratio of sites on the two sublattices and superscripts S1 and S2 indicate the sublattice. Lattice structure (26) represents a reciprocal solution. The molar Gibbs energy according to compound energy formalism is given by equation (28), assuming ideal configurational entropy of mixing within a sublattice and the total entropy is weighed with respect to number of sites on each sublattice.

$$G_{\text{m}} = y_{\text{A}}^{\text{S1}} y_{\text{C}}^{\text{S2}} G_{\text{A:C}}^{\circ} + y_{\text{A}}^{\text{S1}} y_{\text{D}}^{\text{S2}} G_{\text{A:D}}^{\circ} + y_{\text{B}}^{\text{S1}} y_{\text{C}}^{\text{S2}} G_{\text{B:C}}^{\circ} + y_{\text{B}}^{\text{S1}} y_{\text{D}}^{\text{S2}} G_{\text{B:D}}^{\circ} + (mRT(y_{\text{A}}^{\text{S1}} \ln y_{\text{A}}^{\text{S1}} + y_{\text{B}}^{\text{S1}} \ln y_{\text{B}}^{\text{S1}}) + nRT(y_{\text{C}}^{\text{S2}} \ln y_{\text{C}}^{\text{S2}} + y_{\text{D}}^{\text{S2}} \ln y_{\text{D}}^{\text{S2}})) + G^{\text{E}} \quad (28)$$

where G° are Gibbs energies of the end-members, y are constituent fractions and G^E is the excess Gibbs energy expressed with function (29). [26, 27, 36]

$$G^E = y_A^{S1} y_B^{S1} y_C^{S2} L_{A,B:C} + y_A^{S1} y_B^{S1} y_D^{S2} L_{A,B:D} + y_A^{S1} y_C^{S2} y_D^{S2} L_{A,C:D} + y_B^{S1} y_C^{S2} y_D^{S2} L_{B,C:D} + y_A^{S1} y_B^{S1} y_C^{S2} y_D^{S2} L_{A,B:C,D} \quad (29)$$

The excess Gibbs energy function was assumed zero due to small amount of data available and the Gibbs energies of the end-members were optimized based on the experimental data.

4.3.1 CuCl-ZnCl₂

CuCl-ZnCl₂-system is composed of cations having different valences, and therefore requirement for electroneutrality must be taken into consideration. In order to compensate for the charge differences between the cations of the solution, vacant cation sites were added to the model. [25, 36] The CuCl-rich solid solution of the CuCl-ZnCl₂- phase diagram was modelled according to the following sublattice structure (30). [25, 34, 36]



The Gibbs energy of the CuCl-rich solid solution of the CuCl-ZnCl₂-phase diagram was given with Gibbs energies of the following end-member species (31) - (33):



Gibbs energy of the end member $(Cu^+)_1(Cl^-)_1$ represents solid electroneutral compound CuCl and its Gibbs energy of formation is given by equation (34).

$$G_{Cu^+:Cl^-}^{\circ(CuCl)} = G_{CuCl}^{\circ(Solid)} \quad (34)$$

in which $G_{CuCl}^{\circ(Solid)}$ is the Gibbs energy of formation of pure solid CuCl. $(Zn^{2+})_1(Cl^-)_1$ and $(Va)_1(Cl^-)_1$ on the other hand, are charged end-members. The constraint of electroneutrality is satisfied if the site fractions of zinc are equal to the site fractions of vacancies according to (35) ($y_{Zn} = y_{Va}$).



The Gibbs energies of these end-members cannot be obtained experimentally but they can be expressed by the Gibbs energies relative to one chosen charged compound [25, 36]. Gibbs energy for the end-member $(Va)_1(Cl^-)_1$ is thus defined as (36):

$$G_{Va:Cl^-}^{\circ(CuCl)} = \frac{1}{2} G_{Cl_2}^{\circ(gas)} \quad (36)$$

in which $G_{Cl_2}^{\circ(gas)}$ is the Gibbs energy of formation of Cl₂. Now, the Gibbs energy for the end-member $(Zn^{2+})_1(Cl^-)_1$ can be calculated by inserting equations (35) and (36) into equation (37).

$$G_{ZnCl_2}^{\circ(CuCl)} = G_{ZnCl_2}^{\circ(Solid)} + a + bT = G_{Zn^+:Cl^-}^{\circ(CuCl)} + G_{Va:Cl^-}^{\circ(CuCl)} \quad (37)$$

in which $G_{\text{ZnCl}_2}^{\circ(\text{Solid})}$ is the Gibbs energy of formation of pure solid ZnCl_2 and $a+bT$ is a modelling function representing the excess Gibbs energy of the end-member. The resulting Gibbs energy for the end member $(\text{Zn}^{2+})_1(\text{Cl}^-)_3$ is given by equation (38). [36]

$$G_{\text{Zn}^{2+}:\text{Cl}^-}^{\circ(\text{CuCl})} = G_{\text{ZnCl}_2}^{\circ(\text{Solid})} - \frac{1}{2}G_{\text{Cl}_2}^{\circ(\text{gas})} + (a + bT) \quad (38)$$

in which the excess enthalpy term a and the excess entropy term b are solved according to equations (39) and (40).

$$a = H_{\text{Zn}^{2+}:\text{Cl}^-}^{\circ(\text{CuCl})} - H_{\text{ZnCl}_2}^{\circ(\text{Solid})} - \frac{1}{2}H_{\text{Cl}_2}^{\circ(\text{gas})} = H_{\text{Zn}^{2+}:\text{Cl}^-}^{\circ(\text{CuCl})} - H_{\text{ZnCl}_2}^{\circ(\text{Solid})} \quad (39)$$

$$b = S_{\text{Zn}^{2+}:\text{Cl}^-}^{\circ(\text{CuCl})} - S_{\text{ZnCl}_2}^{\circ(\text{Solid})} + \frac{1}{2}S_{\text{Cl}_2}^{\circ(\text{gas})} \quad (40)$$

The solid solution of the ZnCl_2 -rich side of the CuCl - ZnCl_2 phase diagram was not modelled in this work due to the lack of experimental data.

4.3.2 FeCl_3 - ZnCl_2

The solid solution on the FeCl_3 -rich side of the FeCl_3 - ZnCl_2 -phase diagram represents an opposite case compared to the previous copper rich solid solution of the CuCl - ZnCl_2 -system, because the requirement of electroneutrality can be satisfied by formation of vacant sites on the anion sublattice instead of cation sublattice. The iron rich solid solution of the FeCl_3 - ZnCl_2 -phase diagram represents a reciprocal system, which was modelled according to the following sublattice structure (41). [25, 34, 36]

$$(\text{Fe}^{3+}, \text{Zn}^{2+})_1(\text{Va}, \text{Cl}^-)_3 \quad (41)$$

This sublattice structure is composed of the following end-members (42) - (45):

$$(\text{Fe}^{3+})_1(\text{Cl}^-)_3 \quad (42)$$

$$(\text{Fe}^{3+})_1(\text{Va})_3 \quad (43)$$

$$(\text{Zn}^{2+})_1(\text{Cl}^-)_3 \quad (44)$$

$$(\text{Zn}^{2+})_1(\text{Va})_3 \quad (45)$$

End-member $(\text{Fe}^{3+})_1(\text{Cl}^-)_3$ represents solid electroneutral compound FeCl_3 and its Gibbs energy is defined by equation (46).

$$G_{\text{Fe}^{3+}:\text{Cl}^-}^{\circ(\text{FeCl}_3)} = G_{\text{FeCl}_3}^{\circ(\text{Solid})} \quad (46)$$

The rest of the end-members are charged species. Gibbs energy for the charged end-member $(\text{Zn}^{2+})_1(\text{Va})_3$ was defined according to equation (47) and rest of the charged compounds were expressed in relation to its Gibbs energy of formation.

$$G_{\text{Zn}^{2+}:\text{Va}}^{\circ(\text{FeCl}_3)} = G_{\text{ZnCl}_2}^{\circ(\text{Solid})} - G_{\text{Cl}_2}^{\circ(\text{gas})} \quad (47)$$

The electroneutral condition is satisfied by following relation (48).

$$\frac{2}{3}(\text{Zn}^{2+})_1(\text{Cl}^-)_3 + \frac{1}{3}(\text{Zn}^{2+})_1(\text{Va})_3 = \text{Zn}^{2+}\text{Va}(\text{Cl}^-)_2 \quad (48)$$

The Gibbs energies for end-members $(\text{Zn}^{2+})_1(\text{Cl}^-)_3$ and $(\text{Fe}^{3+})_1(\text{Va})_3$ in the FeCl_3 -rich solid solution could be defined by inserting equations (47) and (48) into equation (49), which gives the Gibbs energy for the end-member $(\text{Zn}^{2+})_1(\text{Cl}^-)_3$ according to equation (50).

$$G_{\text{ZnCl}_2}^{\circ(\text{FeCl}_3)} = G_{\text{ZnCl}_2}^{\circ(\text{Solid})} + a + bT = \frac{2}{3}G_{\text{Zn}^{2+}:\text{Cl}^-}^{\circ(\text{FeCl}_3)} + \frac{1}{3}G_{\text{Zn}^{2+}:\text{Va}}^{\circ(\text{FeCl}_3)} + 3RT \left[\frac{2}{3} \ln \left(\frac{2}{3} \right) + \frac{1}{3} \ln \left(\frac{1}{3} \right) \right] \quad (49)$$

$$G_{\text{Zn}^{2+}:\text{Cl}^-}^{\circ(\text{FeCl}_3)} = G_{\text{ZnCl}_2}^{\circ(\text{Solid})} + \frac{1}{2}G_{\text{Cl}_2}^{\circ(\text{gas})} + \frac{3}{2}(a + bT) - 3RT \left[\frac{2}{3} \ln \left(\frac{2}{3} \right) + \frac{1}{3} \ln \left(\frac{1}{3} \right) \right] \quad (50)$$

from which the excess enthalpy term a and the excess entropy term b of the excess Gibbs energy function $a + bT$ of the $(\text{Zn}^{2+})_1(\text{Cl}^-)_3$ end-member can be solved according to equations (51) and (52).

$$a = \frac{2}{3}H_{\text{Zn}^{2+}:\text{Cl}^-}^{\circ(\text{FeCl}_3)} - \frac{2}{3}H_{\text{ZnCl}_2}^{\circ(\text{Solid})} - \frac{1}{2}H_{\text{Cl}_2}^{\circ(\text{gas})} = H_{\text{Zn}^{2+}:\text{Cl}^-}^{\circ(\text{FeCl}_3)} - H_{\text{ZnCl}_2}^{\circ(\text{Solid})} \quad (51)$$

$$b = \frac{2}{3}S_{\text{Zn}^{2+}:\text{Cl}^-}^{\circ(\text{CuCl})} - \frac{2}{3}S_{\text{ZnCl}_2}^{\circ(\text{Solid})} - \frac{1}{3}S_{\text{Cl}_2}^{\circ(\text{gas})} + 3R \left[\frac{2}{3} \ln \left(\frac{2}{3} \right) + \frac{1}{3} \ln \left(\frac{1}{3} \right) \right] \quad (52)$$

Gibbs energy for the end-member $(\text{Fe}^{3+})_1(\text{Va})_3$ can now be solved from the reciprocal reaction (53) by inserting the Gibbs energies of the already solved Gibbs energies of the rest of the end-members (46), (47) and (50).

$$G_{\text{Fe}^{3+}:\text{Va}}^{\circ(\text{FeCl}_3)} + G_{\text{Zn}^{2+}:\text{Cl}^-}^{\circ(\text{FeCl}_3)} = G_{\text{Fe}^{3+}:\text{Cl}^-}^{\circ(\text{FeCl}_3)} + G_{\text{Zn}^{2+}:\text{Va}}^{\circ(\text{FeCl}_3)} \quad \Delta G \quad (53)$$

in which ΔG is the Gibbs energy change of the reciprocal reaction $A + BT$. Solving equation (47) gives Gibbs energy for the end-member $(\text{Fe}^{3+})_1(\text{Va})_3$ according to equation (54). [25, 34]

$$G_{\text{Fe}^{3+}:\text{Va}}^{\circ(\text{FeCl}_3)} = G_{\text{FeCl}_3}^{\circ(\text{Solid})} - \frac{3}{2}G_{\text{Cl}_2}^{\circ(\text{gas})} - \frac{3}{2}(a + bT) + A + BT + 3RT \left[\frac{2}{3} \ln \left(\frac{2}{3} \right) + \frac{1}{3} \ln \left(\frac{1}{3} \right) \right] \quad (54)$$

in which the excess enthalpy term a and the excess entropy term b were solved from equations (55) - (56). When there are no data for an end member of a reciprocal solution and when the end-members are fictitious it is useful to assume that the reciprocal ΔG is zero to avoid reciprocal miscibility gaps [26].

$$a = -\frac{2}{3}H_{\text{Fe}^{3+}:\text{Va}}^{\circ(\text{FeCl}_3)} + \frac{2}{3}H_{\text{FeCl}_3}^{\circ(\text{Solid})} + H_{\text{Cl}_2}^{\circ(\text{gas})} = \frac{2}{3}H_{\text{FeCl}_3}^{\circ(\text{Solid})} - \frac{2}{3}H_{\text{Fe}^{3+}:\text{Va}}^{\circ(\text{FeCl}_3)} \quad (55)$$

$$b = -\frac{2}{3}S_{\text{Fe}^{3+}:\text{Va}}^{\circ(\text{FeCl}_3)} + \frac{2}{3}S_{\text{FeCl}_3}^{\circ(\text{Solid})} + S_{\text{Cl}_2}^{\circ(\text{gas})} + 3R \left[\frac{2}{3} \ln \left(\frac{2}{3} \right) + \frac{1}{3} \ln \left(\frac{1}{3} \right) \right] \quad (56)$$

ZnCl_2 -rich side of the phase diagram was modelled according to following sublattice structure (57). [25, 34]



In which the end-members and their Gibbs energies are defined according to equations (58) - (60):



The end-member $(\text{Zn}^{2+})_1(\text{Cl}^-)_2$ is the solid electroneutral compound ZnCl_2 and its Gibbs energy of formation is given by equation (61).

$$G_{\text{Zn}^{2+}:\text{Cl}^-}^{\circ(\text{ZnCl}_2)} = G_{\text{ZnCl}_2}^{\circ(\text{Solid})} \quad (61)$$

in which $G_{\text{ZnCl}_2}^{\circ(\text{Solid})}$ is the Gibbs energy of formation of pure solid ZnCl_2 . $(\text{Fe}^{3+})_1(\text{Cl}^-)_2$ and $(\text{Va})_1(\text{Cl}^-)_2$ are the charged end-members, for which the requirement of electroneutrality is satisfied by relation (62).

$$(\text{Fe}^{3+})_1(\text{Cl}^-)_2 + \frac{1}{2}(\text{Va})_1(\text{Cl}^-)_2 = \text{Fe}^{3+} + \frac{1}{2}\text{Va}(\text{Cl}^-)_3 \quad (62)$$

Gibbs energies for the vacancy end-member $(\text{Va})_1(\text{Cl}^-)_2$ and the charged $(\text{Fe}^{3+})_1(\text{Cl}^-)_2$ end-member in the ZnCl_2 -rich solid structure can be defined by the following equations (63) and (64).

$$G_{\text{Va}:\text{Cl}^-}^{\circ(\text{ZnCl}_2)} = G_{\text{Cl}_2}^{\circ(\text{gas})} \quad (63)$$

$$G_{\text{FeCl}_3}^{\circ(\text{ZnCl}_2)} = G_{\text{FeCl}_3}^{\circ(\text{Solid})} + a + bT = G_{\text{Fe}^{3+}:\text{Cl}^-}^{\circ(\text{ZnCl}_2)} + \frac{1}{2}G_{\text{Fe}^{3+}:\text{Va}}^{\circ(\text{ZnCl}_2)} + RT \left[\frac{1}{2} \ln \left(\frac{1}{2} \right) \right] \quad (64)$$

By inserting the Gibbs energy for vacancy chloride (63) to equation (62), the Gibbs energy of the $(\text{Fe}^{3+})_1(\text{Cl}^-)_2$ end member is given by equation (65).

$$G_{\text{Fe}^{3+}:\text{Cl}^-}^{\circ(\text{ZnCl}_2)} = G_{\text{FeCl}_3}^{\circ(\text{Solid})} - \frac{1}{2}G_{\text{Cl}_2}^{\circ(\text{gas})} + (a + bT) - RT \left[\frac{1}{2} \ln \left(\frac{1}{2} \right) \right] \quad (65)$$

from which the excess enthalpy term a and the excess entropy term b are solved according to equations (66) and (67). [25, 34]

$$a = H_{\text{Fe}^{3+}:\text{Cl}^-}^{\circ(\text{ZnCl}_2)} - H_{\text{FeCl}_3}^{\circ(\text{Solid})} + \frac{1}{2}H_{\text{Cl}_2}^{\circ(\text{gas})} = H_{\text{Fe}^{3+}:\text{Cl}^-}^{\circ(\text{ZnCl}_2)} - H_{\text{FeCl}_3}^{\circ(\text{Solid})} \quad (66)$$

$$b = S_{\text{Fe}^{3+}:\text{Cl}^-}^{\circ(\text{ZnCl}_2)} - S_{\text{FeCl}_3}^{\circ(\text{Solid})} + \frac{1}{2}S_{\text{Cl}_2}^{\circ(\text{gas})} + R \left[\frac{1}{2} \ln \left(\frac{1}{2} \right) \right] \quad (67)$$

5. Results and Discussion

5.1 The CuCl-ZnCl₂ system

The compositions of the phase boundaries of the CuCl-ZnCl₂-system were measured by annealing the CuCl-ZnCl₂ samples at 230 °C, 240 °C, 250 °C, 300 °C and 340 °C. The results obtained from the EDS-analysis of the quenched samples are shown in table 4 along with standard deviations for both copper and zinc analyses as well as with the total uncertainty for each phase equilibria point calculated based on equation (68).

$$\sigma(\text{total}) = x\text{MCl}_n * \sigma_{\text{M}}\text{MCl}_n + (1 - x\text{MCl}_n) * \sigma_{\text{N}}(1 - x\text{MCl}_n) \quad (68)$$

Where (σ) total is the total uncertainty of the phase equilibria point, σ_{M} and σ_{N} are the standard deviations of the two metals in the system obtained from averages of EDS measurements and $x\text{MCl}_n$ is the average mole fraction of the measured chloride in a phase.

Above 340 °C, the equilibration measurements were not successful due to strong vaporization of the sample. In addition, the experiments done in the ZnCl_2 rich side of the eutectic point of the phase diagram were unsuccessful due vaporization problems, most likely during pre-drying of the sample. The two-phase region in the zinc chloride rich side of the eutectic point is too narrow to allow any cuprous chloride vaporization. The rate of vaporization of the samples was modest during the equilibration at temperatures below 300 °C in the copper-rich side of the eutectic point. Also, due to high cuprous chloride contents and wide solid-liquid phase region in the phase diagram, some cuprous chloride could be vaporized while still retaining

the solid-liquid structure of the sample after quenching. To some extent, stronger vaporization had taken place during the 30 minutes of pre-drying the samples at the 340 °C. This was observed by some analysis points within the sample, where the results of the EDS-analysis showed considerably lower chlorine contents compared to the rest of the sample. These measurements were not taken into consideration for the calculation of the CuCl-ZnCl₂-phase diagram.

Table 4. Summary of the data of the quenched CuCl-ZnCl₂ samples analysed with EDS in mole fractions and the uncertainties (σ) of copper and zinc analyses, which are the standard deviations obtained from the EDS-analysis. (σ) total represents the total uncertainty based on standard deviations according to function $(x_{CuCl} * \sigma_{CuCl}) + (x_{ZnCl_2} * \sigma_{ZnCl_2})$.

solid phase						Liquid phase					
°C	x_{CuCl}	$CuCl(\sigma)$	x_{ZnCl_2}	$ZnCl_2(\sigma)$	(σ) total	°C	x_{CuCl}	$CuCl(\sigma)$	x_{ZnCl_2}	$ZnCl_2(\sigma)$	(σ) total
350±1	0.95	0.028	0.05	0.015	0.027	340±1	0.63	0.021	0.37	0.016	0.019
300±1	0.89	0.042	0.11	0.039	0.042	300±1	0.42	0.082	0.58	0.026	0.050
250±1	0.87	0.04	0.13	0.043	0.040	250±1	0.26	0.034	0.74	0.033	0.033
240±1	0.85	0.025	0.15	0.02	0.024	240±1	0.30	0.019	0.70	0.034	0.029
230±1	0.87	0.031	0.13	0.028	0.031	230±1	0.29	0.023	0.71	0.029	0.027

Copper monochloride vaporizes as a trimer Cu₃Cl₃ (g) and as monomer CuCl (g). The amount of gaseous cuprous chloride starts increasing slowly above 447 - 500 °C and only above 600 °C volatilization of CuCl becomes appreciable [23, 37], whereas ZnCl₂ remains molten below 370 - 400 °C [23, 38]. Above this temperature, molten ZnCl₂ vaporizes rapidly. Below 270 °C, stability of zinc chloride is high but evaporation of ZnCl₂ starts already above 270 -280 °C after which the amount of gas formation increases slowly along with temperature. [38, 39]. This means that fundamentally CuCl should be the more stable component, but surprisingly CuCl was more easily lost from the samples when the temperature was increased. In fact, during equilibration at 350 °C for 20 hours, the liquid phase contained copper rich solid particles that dissolve zinc chloride but the liquid phase contained only ZnCl₂. The cuprous chloride from the liquid had vaporized almost completely.

DeMicco et al. [23] detected that the magnitude of zinc chloride volatilization decreases when other chlorides were present in the system. They studied the effect of copper chloride on the vapour pressure of zinc chloride and found that due to the presence of cuprous chloride, zinc chloride remained in the condensed state possibly through interactions between the gaseous species that form halogen-bridged vapour complexes and because of mutual dissolution of these compounds. It is interesting that these interactions seem to prevent zinc chloride volatilization because interactions with copper chloride changes the zinc chloride properties, but why copper chloride volatilizes at considerably lower temperatures than expected, remains unexplained.

The equilibrium measurements become increasingly difficult as temperature rised because the rate of vaporization increased resulting in inhomogeneous microstructures and increasing loss of material. At temperatures between 300 - 340 °C, too long experiments lead to substantial loss of CuCl, so whether equilibrium is achieved is uncertain in this sense. However, areas in the middle of the sample having repeatable compositions of the liquid were taken into consideration for the calculation of the phase diagram. At 300 °C and above repeatability of the solidus compositions from different experiments was good and equilibrium was achieved in few hours. Solid phase should then reach equilibrium slower due to sluggish solid-state kinetics. Based on this, the liquidus results of the experiments of only couple of hour's duration

could be considered valid, when the parts of the sample, more strongly affected by vaporization, were excluded from the results.

Equilibration and formation of the solid phase seemed to be slow at 230 - 250 °C without pre-treatment at higher temperature. At lower equilibration temperatures, on the other hand, the liquidus compositions were well repeatable and homogenous because of better stability of liquid CuCl and ZnCl₂. Hermann et al. [7] have reported that they could not follow the solidus curve below 340 °C. This is possibly because of slow solid-state kinetics. There seems to be an activation barrier for the solid phase nucleation. When CuCl-ZnCl₂ sample was equilibrated at 300 °C without pre-drying at 340 °C, no solid phase could be found in the sample.

Figure 2 shows typical microstructures of quenched samples of the CuCl-ZnCl₂-system. Figure 2 a represents the microstructure typical to samples equilibrated at 230 – 300 °C containing solid copper rich particles in a porous molten matrix. Figure 2 b represents a micrograph of the CuCl-ZnCl₂-system quenched from 340 °C, where the liquid phase has been dissociated into a eutectic structure during quenching. However, the area analysis taken from the liquid contains the original liquid phase composition.

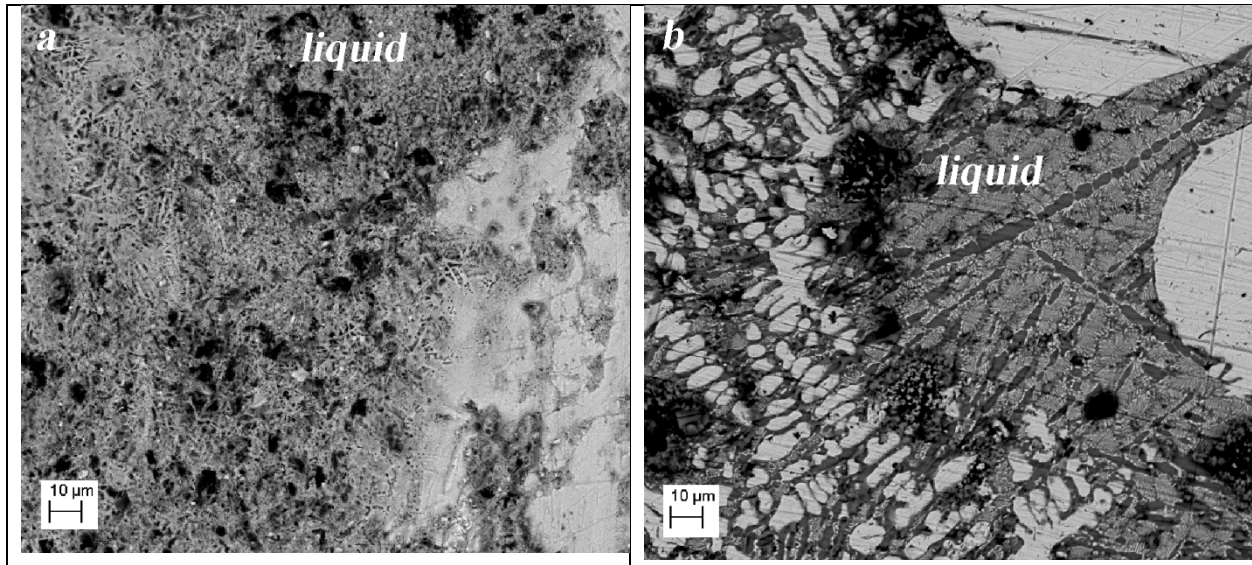


Figure 2. Backscattered scanning electron micrographs of the quenched CuCl-ZnCl₂ samples in argon at 250 °C (a) and 340 °C (b).

The calculated phase diagram of the CuCl-ZnCl₂ system is presented in figure 3 and compared with the existing literature data and the present experimental points. The experimental data by Herrmann et al. [7] from the eutectic point towards the cuprous chloride rich side of the phase diagram and the equilibration/quenching data of the present study was used in the optimization of the CuCl-ZnCl₂-phase diagram in order to find most suitable coefficients for equations (13) and (38). The following parameter values were estimated for the liquid (69) and for the Gibbs energy of the (Zn²⁺)₁(Cl⁻)₁ end member (70) by optimizing the experimental solidus and liquidus data.

$$\Delta g_{\text{Cu}(+)\text{Zn}(2+)/\text{Cl}} \left(\frac{\text{J}}{\text{mol}} \right) = (3960.7 - 3.7732T) - 2018.3x_{\text{Cu}} - (4457.2 - 0.783T)x_{\text{Zn}} \quad (69)$$

$$G_{\text{Zn}^+\text{Cl}^-}^{\circ(\text{CuCl})} \left(\frac{\text{J}}{\text{mol}} \right) = G_{\text{ZnCl}_2}^{\circ(\text{Solid})} - \frac{1}{2} G_{\text{Cl}_2}^{\circ(\text{gas})} + (3165 - 29T) \quad (70)$$

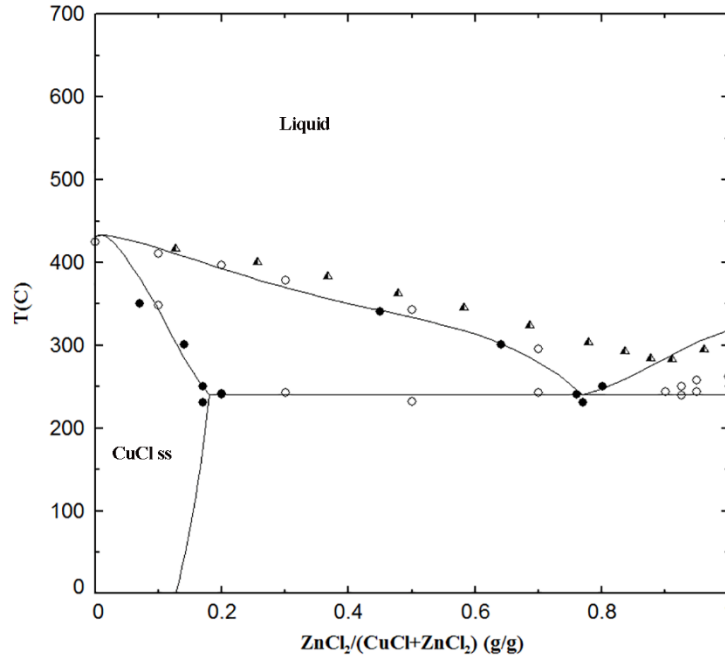


Figure 3. The equilibrium phase diagram of the CuCl-ZnCl₂-system compared with the experimental data. Experimental data are from Herrmann et al [7] (○), Palkin et al [8] (Δ) and this study (●).

The melting temperature of CuCl obtained by Herrmann et al. [7] is in good agreement with the melting temperature of CuCl taken from the FactSage FactPS database. However, the melting temperature of ZnCl₂ by Herrmann et al. is much lower (261.5 °C) than the optimized melting temperature (318 °C) by Robelin et al. [9]. Herrmann et al. [7] reported problems with water absorption of ZnCl₂, which may explain the erroneous melting point, in addition to an undercooling effect of zinc chloride.

ZnCl₂ forms a viscous, polymeric liquid in which Zn²⁺ ions are surrounded tetrahedrally by four chloride ions and each chloride ion is bonded to two zinc ions. The ZnCl₄²⁻ tetrahedrons form a three dimensional network of high viscosity (1121 mPa·s at 350 °C) [40] and low conductivity (1·10⁻³ Ω⁻¹cm⁻¹). [41] Addition of another chloride causes the viscosity of liquid zinc chloride to drop sharply due to breaking of bridging of chloride linkages thus decreasing the degree of polymerization. [42] Viscous melts have smaller thermal and electrical conductivity because increasing number of electrons become localized as a result of directional bonds in liquids exhibiting short-range ordering. [43] Based on this knowledge, the slow reaction kinetics may explain why phase equilibria data in the zinc chloride rich side of the eutectic point has been difficult to measure accurately. For comparison, the viscosity of molten CuCl at 500 °C is only 2.8 mPa·s [40] having electrical conductivity of 3.7 Ω⁻¹cm⁻¹ [41].

In the cuprous chloride-rich side of the CuCl-ZnCl₂-phase diagram, the results of the present experiments agree well with the measurements of Herrmann et al. According to Herrmann et al., the cuprous chloride-rich side of the phase diagram does not require undercooling to crystallize. Also, the effect of water

absorption is less pronounced in the copper rich side because CuCl is not hygroscopic and zinc chloride was dried successfully before the equilibration. Only approximately 3 wt% oxygen concentrations were measured from the samples which is explained by dissolving of SiO₂ from the crucible material and surface oxidation during the sample preparation.

As shown in figure 3, the measured liquidus by Palkin et al. [8] is situated at much higher temperatures compared to the other experimental data, especially at higher zinc chloride concentrations. It is difficult to evaluate why such a difference occurs because the experimental method was not described in their paper, but a high liquidus curve might be explained by moisture and CuCl evaporation from the melt. Based on our SEM micrographs, the sample contained melt still at a temperature as low as 230 °C. This indicates that the measurements by Palkin et al. [8] are likely to give too high liquidus temperatures for the CuCl-ZnCl₂-system. For this reason, the liquidus data of Palkin et al. [8] were not included in the optimization.

Limited solid solubility of ZnCl₂ in CuCl and CuCl in ZnCl₂ exists according to our experiments and as well as according to Herrmann et al. Solid solubility is related to atomic or ionic sizes of the components. According to the Hume-Rothery rule an extensive solid solution is likely to form if the ionic sizes differ less than 15 % [4]. The ionic radiuses of Cu⁺ (0.6 Å with coordination number 2) and Zn²⁺ (0.6 Å with coordination number 4) [44] are the same. However, extent of substitutional solution is determined by other factors as well. If the solute atom differs in valence from the solvent atom, solid solution domain will be limited because structural changes are required in order to preserve the overall electrical neutrality. For example, substitution of a trivalent ion for a divalent ion can be accommodated if an occasional atom site is vacant. The occurrence of complete solubility between end-members requires similar crystal structures. [4] Monovalent cations, such as CuCl, appear to prefer a 2-ligand configuration having a linear structure whereas ZnCl₂ has tetrahedral structure [45].

According to Flengas et al. [45], charge asymmetrical systems often exhibit high exothermic heat effects upon mixing. This applies particularly to systems which approximate the tetrahedral coordination by forming a ACl₄²⁻ complex and in which the complex anions do not dissociate to any appreciable extent. Especially, mixtures of mono- and divalent cations, such as ACl₂-BCl, appear to form complexes with the tetrahedral coordination according to reaction (71). The excess heat of mixing is thought to consist of two parts. Part of the excess enthalpy of mixing originates from a contribution due to formation of a tetrahedrally coordinated anionic ACl₄²⁻ complex. After the formation of this complex, the second part of the enthalpy of mixing arises from the mixing of the complexed species with the unused components in the melt in which the nearest or next nearest coulombic interactions are considered to be significant. [45]



For compositions rich in CuCl the melt microstructure could consist of free CuCl and the complex compound Cu₂ZnCl₄. For compositions rich in ZnCl₂, the melt consists of free ZnCl₂ and the complex compound Cu₂ZnCl₄. The complex ions appear to be more stable in the presence of large cations. If the strength of the complex configuration ACl₄²⁻ is considered to be a result of competing interactions between the A²⁺ and the B⁺ cations for the same chloride anion, the small cations, which create strong electrostatic fields, shall have the tendency to increase the M-Cl bond distance and create weak complexes that may be more prone to dissociation. [45] It is likely that the hypothetical Cu₂ZnCl₄ complex is not stable because Ruthven et al. [35] observed that the liquid systems CuCl₂-CuCl and CuCl₂-CuCl-ZnCl₂ behave

approximately as ideal solutions. Similar observations have been made of other mixtures of a mono- and dihalide such as $\text{BaCl}_2\text{-NaCl}$, $\text{SnCl}_2\text{-CuCl}$ and $\text{PbCl}_2\text{-AgCl}$. If it is assumed that in a mixture of the type $\text{ACl}_2\text{-BCl}$, the number of cation sites is constant over the whole range of composition. This leads to an ideal entropy of mixing and, if it is assumed that the cation-cation interaction is purely electrostatic, the expression for the energy of mixing reduces to zero. [35] This can be the case if the assumed complex ion Cu_2ZnCl_4 is not stable leading to its dissociation causing only small deviations from ideality.

5.2 The $\text{ZnCl}_2\text{-FeCl}_3$ system

The compositions of the phase boundaries of the $\text{FeCl}_3\text{-ZnCl}_2$ -system were measured by annealing the $\text{FeCl}_3\text{-ZnCl}_2$ -samples at 190 °C, 214 °C, 230 °C, and 250 °C. The results obtained from the EDS-analysis are shown in table 5 along with standard deviations for both iron and zinc analyses as well as with the total uncertainty for each phase equilibria point calculated based on equation (68).

Table 5. Summary of the data of the quenched $\text{FeCl}_3\text{-ZnCl}_2$ samples analysed with EDS in mole fractions and the uncertainties (σ) of iron and zinc analyses, which are the standard deviations obtained from the EDS-analysis. (σ) total represents the total uncertainty based on standard deviations according to function $(x\text{FeCl}_3*\sigma_{\text{FeCl}_3})+(x\text{ZnCl}_2*\sigma_{\text{ZnCl}_2})$.

solid phase						Liquid phase					
°C	$x(\text{FeCl}_3)$	FeCl_3 (σ)	$x(\text{ZnCl}_2)$	ZnCl_2 (σ)	(σ) total	°C	$x(\text{FeCl}_3)$	FeCl_3 (σ)	$x(\text{ZnCl}_2)$	ZnCl_2 (σ)	(σ) total
250±1						250±1	0.51	0.013	0.49	0.016	0.014
250±1	0.90	0.043	0.10	0.014	0.040	250±1	0.14	0.013	0.86	0.031	0.028
230±1	0.87	0.1	0.13	0.029	0.013	230±1	0.45	0.035	0.55	0.03	0.032
230±1	0.08	0.017	0.92	0.031	0.030	230±1	0.18	0.015	0.82	0.024	0.022
214±1	0.08	0.022	0.92	0.045	0.043	214±1	0.27	0.046	0.73	0.041	0.038
214±1	0.71	0.022	0.29	0.023	0.022	214±1	0.42	0.034	0.58	0.038	0.036
190±1	0.11	0.018	0.89	0.017	0.017	190±1	0.29	0.049	0.71	0.044	0.045

FeCl_3 is volatilized above 250 °C mostly as two species Fe_2Cl_6 (g) and Cl_2 (g) [22, 46]. The temperature range of the liquidus curve of the $\text{ZnCl}_2\text{-FeCl}_3$ -system is so low that pre-drying of the samples was not possible, which lead to presence of some crystalline water within the samples. This was sometimes seen as disappearance of one phase domain under the electron beam during scanning electron microscopy. The fact that the samples were not pre-dried and pre-melted at higher temperatures might be connected to appearance of strange microstructure found in the iron rich side of the phase diagram, shown in figure 4 a, since enough energy for the activation for nucleation of the solid phase might not have been achieved. In addition, a higher water absorption from the ambient air might affect the fact that typical solid-liquid microstructure never formed during equilibration. A similar effect was observed during one experiment of the $\text{CuCl}\text{-ZnCl}_2$ -system conducted without pre-drying with ammonium chloride at 340 °C. Despite of these difficulties, different chemical compositions were found in the samples, which were repeatable and match with the results of Hermann et al. within the iron chloride rich side of the phase diagram. These data points could be interpreted as solid and liquid despite the unconventional appearance in the microstructure.

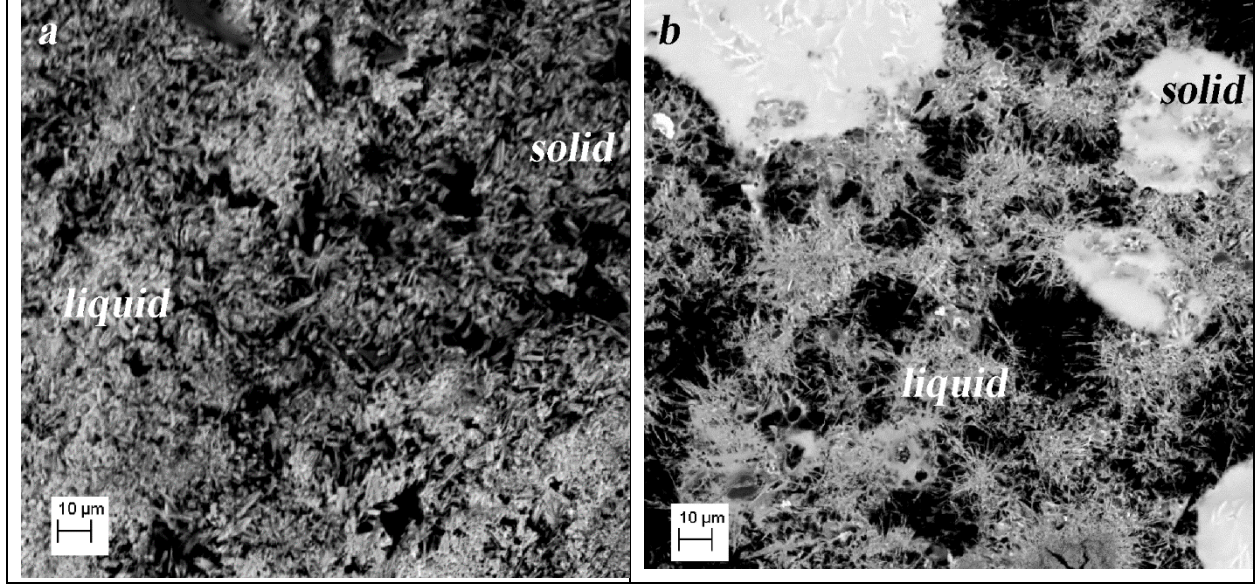


Figure 4. Backscattered scanning electron micrographs of the quenched $\text{FeCl}_3\text{-ZnCl}_2$ samples at 230 °C, (a) representing the FeCl_3 -rich sample and (b) representing the ZnCl_2 -rich sample.

Despite staying below 250 °C during the equilibration experiments, FeCl_3 vaporization resulted in formation of a structure where the upper part of the sample contained typically two different iron-rich phases, as vapours of iron chloride were transported upwards from the bottom of the crucible replacing the iron chloride lost to the gas phase. As a result, the lower part of the sample was depleted of FeCl_3 changing the composition towards the two phase region of the zinc chloride rich side of the phase diagram and resulting in similar phase compositions obtained in the experiments done in the zinc chloride rich side of the $\text{FeCl}_3\text{-ZnCl}_2$ -phase diagram. Thus, the lower section of the sample has most likely been equilibrated within the two-phase region of the zinc chloride-rich side of the eutectic point for a while, until the quenching resulting in a microstructure similar to that shown in figure 4 b. Unfortunately, because of this type of problem it is difficult to be sure, whether equilibrium is achieved since, the extent of FeCl_3 vaporization was dependent on the equilibration time and temperature. The samples that were equilibrated in the zinc chloride rich side of the phase diagram contained mostly zinc chloride and only very few areas on the side walls of the crucible contained solutions of iron and zinc chloride. As proved by deMicco et al. [22], interactions between chlorides can lead to vaporization, which may be different from what is predicted. Too long experiments done with too small iron chloride concentrations even at the lower experimental temperatures (214 °C), resulted in a samples of pure zinc chloride.

The calculated phase diagram of the $\text{FeCl}_3\text{-ZnCl}_2$ system is presented in figure 5 and compared with the existing literature data by Herrmann et al. [7] and the present experimental data. The following parameters according to equations (13), (50), (54) and (65) were obtained for the Gibbs energy of the liquid (72) and for the Gibbs energies of the $(\text{Fe}^{3+})_1(\text{Va})_3$ (73), $(\text{Zn}^{2+})_1(\text{Cl}^-)_3$ (74) and $(\text{Fe}^{3+})_1(\text{Cl}^-)_2$ (75) end members.

$$\Delta g_{\text{Fe}(3+)\text{Zn}(2+)/\text{Cl}} \left(\frac{\text{J}}{\text{mol}} \right) = -3865 + 634 x_{\text{Fe}} - 5687 x_{\text{Zn}} \quad (72)$$

$$G_{\text{Zn}^{2+}:\text{Cl}^-}^{\circ(\text{FeCl}_3)} \left(\frac{\text{J}}{\text{mol}} \right) = G_{\text{ZnCl}_2}^{\circ(\text{Solid})} + \frac{1}{2} G_{\text{Cl}_2}^{\circ(\text{gas})} + \frac{3}{2} (7455 - 17T) - 3RT \left[\frac{2}{3} \ln \left(\frac{2}{3} \right) + \frac{1}{3} \ln \left(\frac{1}{3} \right) \right] \quad (73)$$

$$G_{\text{Fe}^{3+}:\text{Va}}^{\circ(\text{FeCl}_3)} \left(\frac{\text{J}}{\text{mol}} \right) = G_{\text{FeCl}_3}^{\circ(\text{Solid})} - \frac{3}{2} G_{\text{Cl}_2}^{\circ(\text{gas})} - \frac{3}{2} (7455 - 17T) + 3RT \left[\frac{2}{3} \ln \left(\frac{2}{3} \right) + \frac{1}{3} \ln \left(\frac{1}{3} \right) \right] \quad (74)$$

$$G_{\text{Fe}^{3+}:\text{Cl}^-}^{\circ(\text{ZnCl}_2)} \left(\frac{\text{J}}{\text{mol}} \right) = G_{\text{FeCl}_3}^{\circ(\text{Solid})} - \frac{1}{2} G_{\text{Cl}_2}^{\circ(\text{gas})} + (6756 - 12T) - RT \left[\frac{1}{2} \ln \left(\frac{1}{2} \right) \right] \quad (75)$$

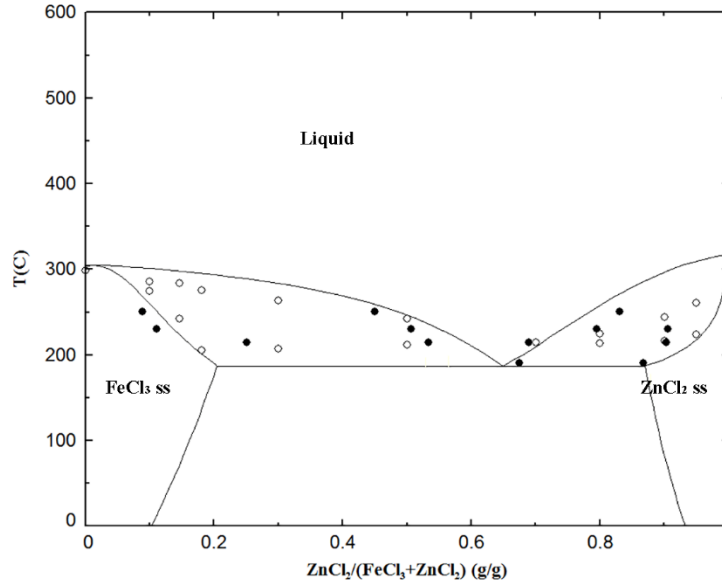


Figure 5. The equilibrium phase diagram of the FeCl_3 - ZnCl_2 -system compared with experimental results. Experimental data are from Herrmann et al [7] (○) and this study (●).

Herrmann et al. [7] reported their measured eutectic temperatures scatter between 205 °C - 216 °C and they increased with increasing zinc chloride concentration. They also observed that the FeCl_3 - ZnCl_2 -system between compositions of 18 wt% - 70 wt% of ZnCl_2 requires an undercooling of 4 °C – 10 °C to crystallize. Due to the polymeric ZnCl_4^{2-} -structure of molten zinc chloride, the viscosity of the melt is likely to increase as zinc chloride concentration increases. This may explain the rising trend of eutectic crystallization temperature as a function of increasing zinc chloride concentration. Liquids with higher viscosities tend to have slower reaction rates, since absorption of heat in the melt becomes slower as the viscosity increases [4]. Also, different levels of crystalline water within the samples explain why Herrmann et al. [7] had difficulties in measuring the eutectic temperature, since both components are hygroscopic and form various hydrates. Unfortunately, this uncertainty could not be improved by our experiments.

For a material that readily crystallizes from its molten phase, cooling curves can be quite suitable for phase diagram studies. However, if the system requires undercooling to crystallize the phase transition is typically detected at lower temperatures than the equilibrium value [4, 18]. Crystallization from high viscosity liquids proceeds with difficulty, and accordingly, since attainment of equilibrium under such conditions requires excessively long periods of time, the cooling curve methods are likely to yield erroneous results. Heating curves although not impeded by undercooling difficulties, also suffer from this sluggishness of reactions in systems containing viscous liquids. The heat effects, absorption or evolution of heat, which indicate phase changes in the heating or cooling curves, are not easily defined in such systems where reactions are slow. [4]

Contrary to other trivalent chlorides, FeCl₃ shows relatively good ionic conductivity (0.04 Ω⁻¹cm⁻¹), which arises from a more closely packed molecular melt allowing transfer of halogen ions between neighbouring molecular units, such as Fe₂Cl₆ and Fe₂Cl₇⁻. [47] However, the ionic conductivity of molten iron chloride is considerably lower compared to many chlorides, such as e.g. CuCl (3.7 Ω⁻¹cm⁻¹). The slow interactions between ZnCl₂ and FeCl₃ could be explained by considering somewhat out of the ordinary melting behaviour of the two chlorides. ZnCl₂ melts to form a polymeric network of very low ionic conductivity and very high viscosity. This combined with low ionic conductivity of FeCl₃, which forms a Fe₂Cl₆-structured molecular liquid during melting might explain the difficulties of interactions between these components.

As observed by the scanning electron microscopy, nucleation and equilibration of the solid solution phase is difficult due to slow kinetics (such as nucleation barrier) of reactions during equilibration. Larger solubilities were measured by equilibration/quenching method in the solid zinc chloride rich side of the phase diagram compared to the heating and cooling curve measurements by Herrmann et al. [7], probably due to slow kinetics of the equilibration of the solid phase as longer annealing times were used for the equilibration. Even though, the solute ion differs in valence from the solvent ion, the ionic radiuses of Zn²⁺ 0,6 Å (coordination number 4) and Fe³⁺ 0.65 Å (coordination number 6) are very close to each other in size [44]. Thus, a substitutional solid solution in both sides of the phase diagram is likely to exist [9], which, was confirmed by the measurements of this study as well as by Herrmann et al. [7] Although, for systems where viscosity is low, as with liquid salts in general, the heating and cooling curves are an applicable approach to measure phase transition temperatures. The quenching method is better suited for sluggish reaction kinetics due to longer annealing times. This way the quenching method locates more accurately the phase transition compositions in those systems that are slow to crystallize. [4] This is likely to be more true in case of the measured solid solution compositions because vaporization from the liquid phase brings inaccuracy to the liquidus measurements.

5.3 The CuCl-FeCl₃ system

The compositions of the phase boundaries of the CuCl-FeCl₃-system were measured by annealing the samples at 307 °C, and 350 °C. The results obtained from the EDS-analysis of the quenched samples are shown in table 6 along with standard deviations for both copper and iron analyses as well as with the total uncertainty for each phase equilibria point calculated based on equation (68).

Table 6. Summary of the data of the quenched CuCl-FeCl₃ samples analysed with EDS in mole fractions and the uncertainties (σ) of copper and iron analyses, which are the standard deviations obtained from the EDS-analysis. (σ) total represents the total uncertainty based on standard deviations according to function $(x_{\text{CuCl}} \cdot \sigma_{\text{CuCl}}) + (x_{\text{FeCl}_3} \cdot \sigma_{\text{FeCl}_3})$.

solid phase						Liquid phase					
°C	$x(\text{CuCl})$	$(\sigma)\text{CuCl}$	$x(\text{FeCl}_3)$	$(\sigma)\text{FeCl}_3$	$(\sigma) \text{ total}$	°C	$x(\text{CuCl})$	$(\sigma)\text{CuCl}$	$x(\text{FeCl}_3)$	$(\sigma)\text{FeCl}_3$	$(\sigma) \text{ total}$
350±1	0.99	0.039	0.01	0.002	0.039	350±1	0.76	0.024	0.24	0.008	0.020
307±1	0.98	0.008	0.02	0.009	0.008	307±1	0.64	0.034	0.36	0.017	0.031
307±1	0.98	0.01	0.02	0.008	0.010	307±1	0.58	0.029	0.42	0.034	0.023

Figure 5 shows microstructure examples of the quenched samples of the CuCl-FeCl₃-system. Figure 6 a represents the microstructure typical to samples equilibrated at 307 °C containing solid copper chloride particles surrounded by the liquid. Figure 6 b represents a SEM micrograph of the CuCl-FeCl₃-system quenched from 350 °C, where the liquid phase has been separated into a eutectic structure during quenching. However, EDS area analysis taken from the liquid contains the original liquid phase composition.

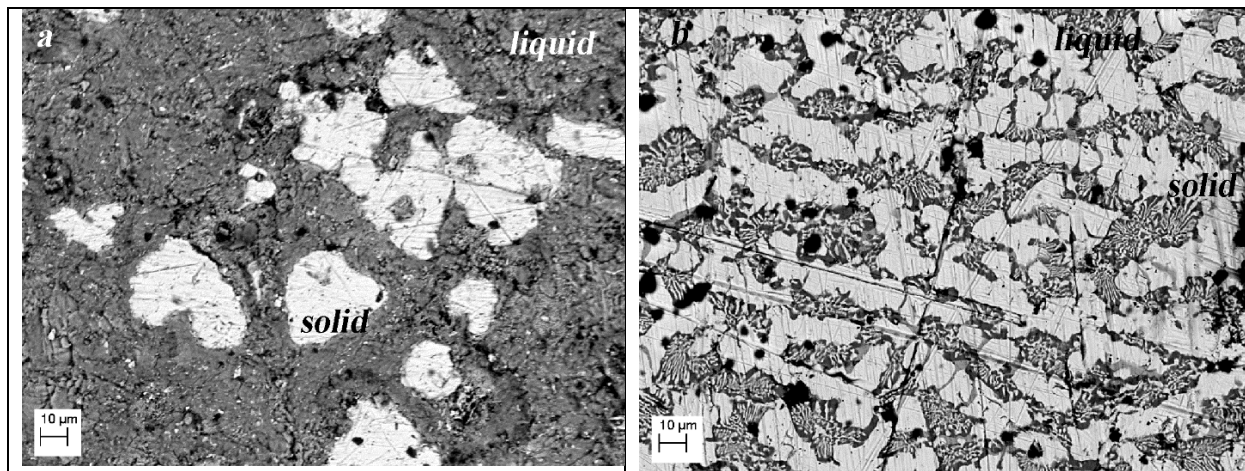


Figure 6. Backscattered scanning electron micrographs of the quenched CuCl-FeCl₃ samples at 307 °C (a) and 350 °C (b).

The CuCl-FeCl₃-phase diagram differs from the previous CuCl-ZnCl₂ and FeCl₃-ZnCl₂ systems so that no significant terminal solid solutions are formed. Instead, a double chloride (Cu₂Cl₂(FeCl₃)₂) observed by Herrmann et al. [7] is formed at the composition of 62 wt% of CuCl. In the optimization of the CuCl-CuCl₂-FeCl₂-FeCl₃, the postulated CuFeCl₄ phase was not included. Instead, the optimized phase equilibria showed similar behaviour even if no intermediate CuFeCl₄ existed due to the multicomponent nature of the system. Since the crystal structures of CuCl (linear) and FeCl₃ (octahedral) are different, a complete solid solubility is not possible. If however, there are strong chemical affinity between the two kinds of atoms, a more stable configuration may be attained by the formation of a compound. In this case, solid solubility would be restricted to small concentrations. [4]

The CuCl-FeCl₃-system may contain Cu⁺, Cu²⁺, Fe²⁺, and Fe³⁺ in the liquid phase and the liquid phase should be considered to be composed of pseudo-binary systems. For proper description of the thermodynamic properties, the true binaries CuCl-CuCl₂, and FeCl₂-FeCl₃ were included and optimized assuming no metal (Fe or Cu) or Cl₂ dissolution in the melt. The systems CuCl-FeCl₂ and CuCl₂-FeCl₃ represent the reduced and oxidized quasibinary systems, respectively. The optimized CuCl-FeCl₃ phase diagram is shown in figure 7d and the optimized CuCl₂-FeCl₂ phase diagram shown in figure 7c represent ternary sections in the Cu-Fe-Cl system. The interactions in the CuCl-FeCl₂ and CuCl₂-FeCl₃ systems were not included in the optimizations due to the lack of experimental data for these sections.

The calculated phase diagram of the CuCl-FeCl₃-system is presented in figure 7 d and compared with the existing literature data by Herrmann et al. [7] and data from the present experimental work. The CuCl-FeCl₃-system does not require undercooling to crystallize, has a low viscosity and could be pre-dried before

the equilibration annealing. Lack of these uncertainties are likely to explain the good agreement between the results of this study and the results of Herrmann et al. [7] The following parameters (76) – (79) for the excess Gibbs energy of the liquid phase according to equation (13) and (25) were obtained for the Gibbs energy of the liquid phase. Non-ideal behaviour of the FeCl₂-FeCl₃ system (figure 7b) was optimized using the phase diagram data by Schäfer et al. [15] and the FeCl₂-CuCl₂ system (figure 7c) was optimized using the phase diagram data by Korzhukov et al. [16].

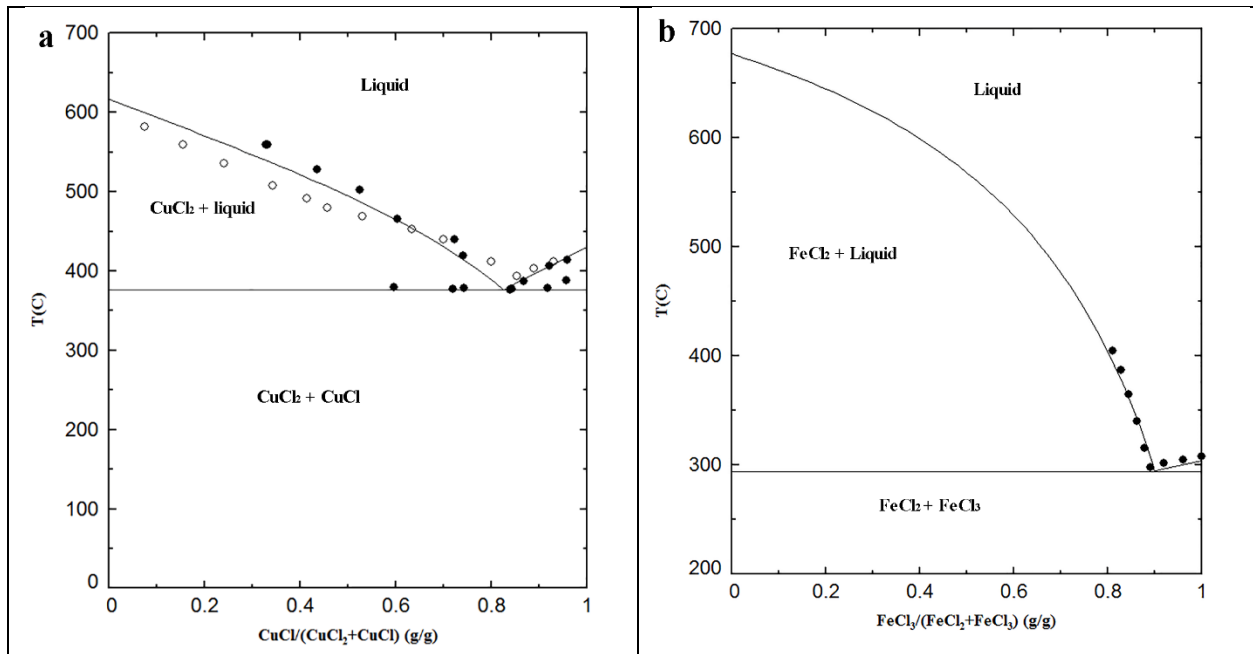
$$\Delta g_{\text{Cu}(+)\text{Fe}(3+)/\text{Cl}} \left(\frac{\text{J}}{\text{mol}} \right) = -4364 + (2940 + 3.24T)x_{\text{Cu}} - 1534 x_{\text{Fe}} \quad (76)$$

$$\Delta g_{\text{Fe}(3+)\text{Fe}(2+)/\text{Cl}} \left(\frac{\text{J}}{\text{mol}} \right) = -4855 + 4.19T \quad (77)$$

$$\Delta g_{\text{Fe}(2+)\text{Cu}(2+)/\text{Cl}} \left(\frac{\text{J}}{\text{mol}} \right) = -2191 \quad (78)$$

CuCl melts at 424 °C, and CuCl₂ melts at around 600-650 °C, but due to decomposition of CuCl₂ to CuCl and Cl₂, it is difficult to assess the melting point of CuCl₂. In the present study, the metastable melting point of CuCl₂ was optimized. The CuCl-CuCl₂ phase diagram (figure 7a) was optimized using the phase diagram data by Bilzt et al. [13] and Safonov et al. [14] The following Gibbs energy equation (79) was obtained for the melting of CuCl₂ according to equation (25).

$$G_{\text{CuCl}_2}^{\circ(\text{Liquid})} \left(\frac{\text{J}}{\text{mol}} \right) = G_{\text{CuCl}_2}^{\circ(\text{Solid})} + (40000 - 45T) \quad (79)$$



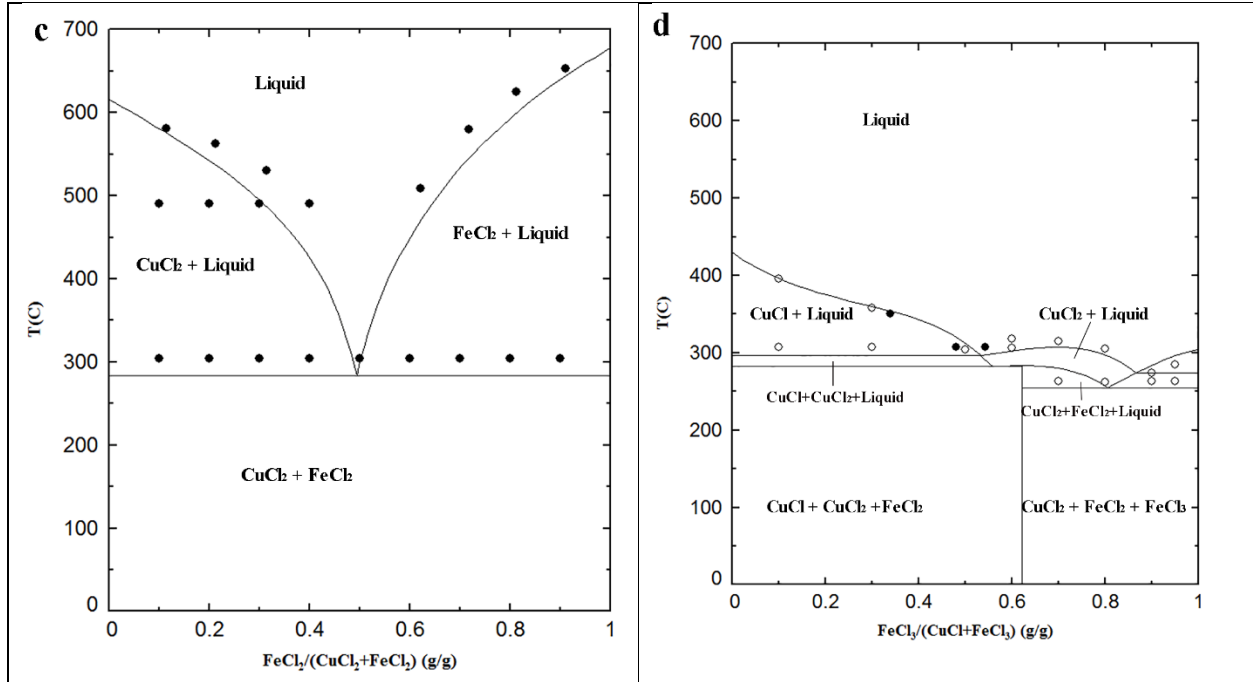


Figure 7. The equilibrium phase diagram of the $\text{CuCl}_2\text{-CuCl}$, $\text{FeCl}_2\text{-FeCl}_3$, $\text{CuCl}_2\text{-FeCl}_2$ and CuCl-FeCl_3 -systems compared with experimental data. Experimental data in figure a are from Biltz et al. [13] (\circ) and Safonov et al. [14] (\bullet). Experimental data in figure b are from Schäfer et al. [15] (\bullet). Experimental data in figure c are from Korzhukov et al. [16] (\bullet). Experimental data in figure d are from this study (\bullet) and from Herrmann et al. [7] (\circ).

5.4 CuCl-PbCl_2

The two studies of CuCl-PbCl_2 phase equilibria by Herrmann et al. [7] and Coleman et al. [17] show similar results for the solidus temperature, but the measured liquidus temperature in the study of Coleman et al. [17] is lower than that of Herrmann et al. [7]. Coleman et al. [17] reported an uncertainty in the measurements of $\pm 30^\circ\text{C}$. The liquidus data of Herrmann et al. [7] gives more reasonable results for the optimization of the liquidus data, and the optimization is mainly based on these data. The optimized parameter according to equation (13) for the liquid is given in equation (80). The optimized phase diagram of CuCl-PbCl_2 together with the experimental points is shown in Figure 8.

$$\Delta g_{\text{Cu}(+)\text{Pb}(2+)/\text{Cl}} \left(\frac{\text{J}}{\text{mol}} \right) = -360.8 - 798.8x_{\text{Pb}(2+)} \quad (80)$$

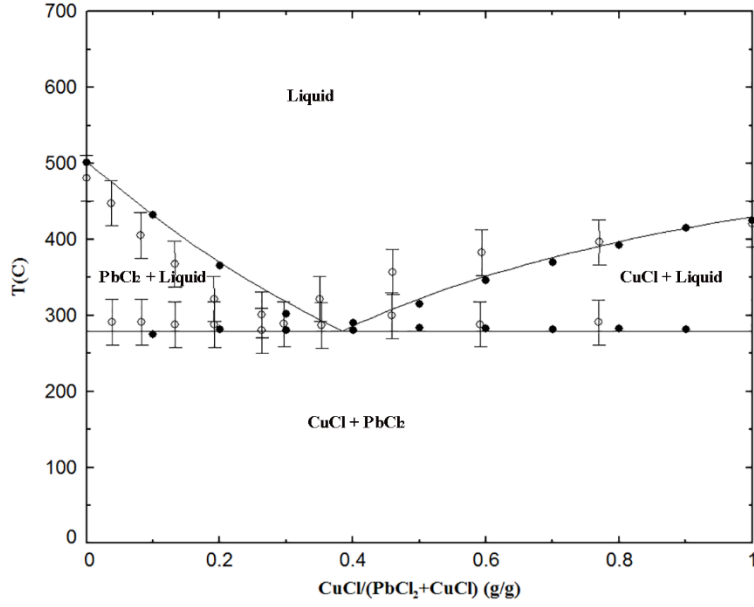


Figure 8. Equilibrium phase diagram of the CuCl-PbCl₂-system compared with experimental results. Experimental data are from Hermann et al. [7] (●) and from Coleman et al. [17] (○) with uncertainty bars included.

5.5 Summary of optimized results

In the present study, the thermodynamic interaction parameters for the liquid phase was optimized based on the experimental data from the literature and our own experimental data. The thermodynamic data for liquid CuCl₂ was also optimized as follows:

$$G_{\text{CuCl}_2}^{\circ(\text{Liquid})} / \left(\frac{\text{J}}{\text{mol}} \right) = G_{\text{CuCl}_2}^{\circ(\text{Solid})} + (40000 - 45T) \quad (79)$$

The optimized interaction parameters for the liquid phase according to the quasi-chemical model are given in table 7 and the Gibbs energies for the end-members of the solid phases according to compound energy formalism are given in table 8. The calculated eutectic points for the binary systems are shown in Table 9.

Table 7. Optimized interaction parameters for the liquid phase

Interaction parameters	
CuCl-ZnCl ₂	
$\Delta g_{\text{Cu}(+)\text{Zn}/\text{Cl}} / (\text{J/mol}) = 3960.7 - 3.773T - 2018.3x_{\text{Cu}(+)} - (4457.2 - 0.783T)x_{\text{Zn}}$	
FeCl ₃ -ZnCl ₂	
$\Delta g_{\text{Fe}(3+)\text{Zn}/\text{Cl}} / (\text{J/mol}) = -3865 + 634 x_{\text{Fe}(3+)} - 5687x_{\text{Zn}}$	
CuCl-FeCl ₃	
$\Delta g_{\text{Fe}(2+)\text{Fe}(3+)/\text{Cl}} / (\text{J/mol}) = -4855 + 4.19T$	
$\Delta g_{\text{Cu}(2+)\text{Fe}(2+)/\text{Cl}} / (\text{J/mol}) = -2191.38$	
$\Delta g_{\text{Cu}(+)\text{Fe}(3+)/\text{Cl}} / (\text{J/mol}) = -4364 + (2940 + 3.24T)x_{\text{Cu}(+)} - 1534x_{\text{Fe}(3+)}$	

CuCl-PbCl ₂
$\Delta g_{\text{Cu}^{+}\text{Pb}/\text{Cl}} / (\text{J/mol}) = -360.8 - 798.8x_{\text{Pb}(2+)}$

Table 8. Gibbs energies for the solid phase end-members including optimized Gibbs energies for the charged end-members (Zn⁺Cl⁻), (Zn²⁺Cl⁻), (Fe³⁺Va) and (Fe³⁺Cl⁻).

Gibbs energies for the solid phase end-members	
CuCl-ZnCl₂	
$G_{\text{Cu}^{+}\text{Cl}^{-}}^{\circ(\text{CuCl})} / (\text{J/mol}) = G_{\text{CuCl}}^{\circ(\text{Solid})}$	
$G_{\text{Va:Cl}^{-}}^{\circ(\text{CuCl})} / (\text{J/mol}) = \frac{1}{2} G_{\text{Cl}_2}^{\circ(\text{gas})}$	
$G_{\text{Zn}^{+}\text{Cl}^{-}}^{\circ(\text{CuCl})} / \left(\frac{\text{J}}{\text{mol}}\right) = G_{\text{ZnCl}_2}^{\circ(\text{Solid})} - \frac{1}{2} G_{\text{Cl}_2}^{\circ(\text{gas})} + (3165 - 29T)$	
FeCl₃-ZnCl₂	
FeCl₃ rich solid solution	
$G_{\text{Fe}^{3+}\text{Cl}^{-}}^{\circ(\text{FeCl}_3)} / (\text{J/mol}) = G_{\text{FeCl}_3}^{\circ(\text{Solid})}$	
$G_{\text{Zn}^{2+}\text{Va}}^{\circ(\text{FeCl}_3)} / (\text{J/mol}) = G_{\text{ZnCl}_2}^{\circ(\text{Solid})} - G_{\text{Cl}_2}^{\circ(\text{gas})}$	
$G_{\text{Zn}^{2+}\text{Cl}^{-}}^{\circ(\text{FeCl}_3)} / (\text{J/mol}) = G_{\text{ZnCl}_2}^{\circ(\text{Solid})} + \frac{1}{2} G_{\text{Cl}_2}^{\circ(\text{gas})} + \frac{3}{2}(7455 - 17T) - 3RT \left[\frac{2}{3} \ln \left(\frac{2}{3}\right) + \frac{1}{3} \ln \left(\frac{1}{3}\right) \right]$	
$G_{\text{Fe}^{3+}\text{Va}}^{\circ(\text{FeCl}_3)} / (\text{J/mol}) = G_{\text{FeCl}_3}^{\circ(\text{Solid})} - \frac{3}{2} G_{\text{Cl}_2}^{\circ(\text{gas})} - \frac{3}{2}(7455 - 17T) + 3RT \left[\frac{2}{3} \ln \left(\frac{2}{3}\right) + \frac{1}{3} \ln \left(\frac{1}{3}\right) \right]$	
ZnCl₂ rich solid solution	
$G_{\text{Zn}^{2+}\text{Cl}^{-}}^{\circ(\text{ZnCl}_2)} / (\text{J/mol}) = G_{\text{ZnCl}_2}^{\circ(\text{Solid})}$	
$G_{\text{Va:Cl}^{-}}^{\circ(\text{ZnCl}_2)} / (\text{J/mol}) = G_{\text{Cl}_2}^{\circ(\text{gas})}$	
$G_{\text{Fe}^{3+}\text{Cl}^{-}}^{\circ(\text{ZnCl}_2)} / \left(\frac{\text{J}}{\text{mol}}\right) = G_{\text{FeCl}_3}^{\circ(\text{Solid})} - \frac{1}{2} G_{\text{Cl}_2}^{\circ(\text{gas})} + (6746 - 12T) - RT \left[\frac{1}{2} \ln \left(\frac{1}{2}\right) \right]$	

Table 9. Calculated eutectic points of the optimized phase diagrams in mole fractions.

CuCl-ZnCl ₂	$x(\text{ZnCl}_2) = 0.71$; T = 241°C
FeCl ₃ -ZnCl ₂	$x(\text{ZnCl}_2) = 0.69$; T = 182°C
CuCl-FeCl ₃	$x(\text{FeCl}_3) = 0.41$; T = 295 °C, $x(\text{FeCl}_3) = 0.8$; T = 275 °C
FeCl ₂ -FeCl ₃	$x(\text{FeCl}_3) = 0.88$; T = 295 °C
CuCl-CuCl ₂	$x(\text{CuCl}) = 0.87$; T = 377 °C
CuCl ₂ -FeCl ₂	$x(\text{FeCl}_2) = 0.5$; T = 285°C
CuCl-PbCl ₂	$x(\text{CuCl}) = 0.636$; T = 278.8°C

6. Conclusions

The thermodynamic properties of the CuCl-ZnCl₂, FeCl₃-ZnCl₂, CuCl-FeCl₃ and CuCl-PbCl₂-systems were assessed using the CALPHAD technique. The modified quasi-chemical model was used for describing the molten chloride solutions and the compound energy formalism for the solid chloride solutions. The model parameters that describe satisfactorily the experimental data available were derived by the optimizations carried out in this work.

The Gibbs energies of cation-cation pair formations for the two different cations in each binary were negative indicating the tendency of the liquid phase to become more ordered. The excess enthalpies of mixing of the solid solutions of the CuCl-ZnCl₂ and FeCl₃-ZnCl₂ systems had positive deviations from the ideality.

Because of the lack of thermodynamic data of these systems, new equilibration, quenching and scanning electron microscopy EDS observations were done to supplement the scarce existing data for the modelling. The equilibration and quenching method in open containers is not fully suitable for measuring the phase equilibria of these chloride systems in the highest temperature ranges of the phase diagrams, due to strong vaporization effects. Instead, the method may be completely suitable for measuring phase equilibria at lower temperature ranges of the phase diagrams, especially in systems containing zinc chloride. The vaporization tendency is possible to eliminate with closed containers and by handling the sample materials in a clove box. The CuCl-ZnCl₂ and FeCl₃-ZnCl₂-systems seem to require higher energies achieved by pre-melting and longer equilibration times in order to exceed the energy barrier needed for the nucleation of the solid phase. Systems containing zinc chloride are also likely to be more viscous than molten salts otherwise, due to the polymeric structure of ZnCl₂, thus requiring longer annealing times to equilibrate. The solid solubilities of the CuCl-ZnCl₂ and FeCl₃-ZnCl₂-systems were completed with the equilibration quenching method providing new experimental data that could not have been obtained before using the method of heating and cooling curves. New experimental data are still required to develop a better description of the studied systems. Especially more reliable experimental data are needed for the FeCl₃-ZnCl₂-system and the ternaries. Also further studies connecting the developed thermodynamic database with other chloride species, such as KCl, and NaCl, as well as metal sulfates are recommended.

Acknowledgements

This work was financed by Eemil Aaltonen Foundation and by Walter Ahlström Foundation.

Declaration of interest: none

Data availability statement

The raw data required to reproduce these findings are included in this manuscript. The raw data is provided in tables 4, 5 and 6 and the experimental phase equilibria points are averages of the EDS-results of the equilibrated and quenched samples at each equilibration temperature. About 30 EDS measurements have been taken from both the liquid and solid phases and for this reason the standard deviations showing the measurement uncertainty for each metal separately and for the total uncertainty of each phase equilibria point are also provided in tables 4, 5 and 6.

References

1. E. Miettinen, Thermal conductivity and characteristics of copper flash smelting flue dust accretions, *Doctoral thesis*, Helsinki University of Technology (2008), 1-38.
2. Hanna Viitala, Pekka Taskinen, Hot corrosion mechanism of steels exposed to heavy metal chlorides and sulphates in SO₂-environment, *Oxid. Met.*, 86 (2016), 239 - 262.
3. Hanna Viitala, Pekka Taskinen, Influence of nickel alloying on hot-corrosion of stainless steels in SO₂-environment, *Mater. Sci. Technol.*, 33 (2017) 49 – 64.
4. C.G. Bergeron, S.H. Risbud, Introduction to Phase Equilibria in Ceramics, The American Ceramic Society, Inc, Columbus (OH), 2 edition (1984) 1- 6, 32 – 38.
5. E.Haccuria, T. Grivits, P.C. Hayes, E. Jak, Selected Phase Equilibria Studies in the Al₂O₃-CaO-SiO₂ System, *J. Am. Ceram. Soc.* 99 (2016) 691-704.
6. E. Jak, Integrated experimental and thermodynamic modelling research methodology for metallurgical slags with examples in the copper production field, *Int.Symp.Molten*, Beijing, (2012) 1-21.

7. G. Herrmann, Über die Verbindungsfähigkeit der Chloride von Cu, Pb, Fe, Zn, Sn und Bi, *Z. Anorg. Chem.* 71 (1911) 257 – 302.
8. A. P. Palkin, G. P. Chepurko, The reaction of salts with metals in the molten state. The reaction of CuCl with zinc, *Zh. Neorg. Khim.* 8 (1956), 1833-1842.
9. C. Robelin, P.J. Chartrand, Thermodynamic evaluation of and optimization of the (NaCl+KCl+MgCl₂+ZnCl₂) system, *J. Chem. Thermodynam.* 43 (2011), 377-391.
10. C. W. Bale, E. Bélisle, P. Chartrand, S. A. Decterov, G. Eriksson, A. E. Gheribi, M. A. Van Ende, FactSage thermochemical software and databases, *Calphad*, 54 (2016), 35-53.
11. J. Meyer, J. Korb, K. Hein, Dampfdruckuntersuchungen im System ZnCl₂-CuCl, *Neue Hütte*, 34 (1989) 185 – 188.
12. E.G. Kozachenko, V.V. Safonov, N.A. Levina, V.I. Ksenzenko, Equilibrium Diagrams of the BiCl₃-CuCl-TeCl₄ and CuCl-FeCl₃-TeCl₄ Systems, *Zh. Neorg. Khim.* 21 (1976) 219-221.
13. W. Biltzt, W. Fischer, Beiträge zur systematischen Verwandtschaftslehre über das System Cupro-/Cuprichlorid, Hannover, Technische Hochschule, Institut für anorganische Chemie. (1927) 290 - 299.
14. V.V. Safonov, V.A. Mireiev, S.K. Dubina, D.V. Baiandin, *Z. Neorg. Chim.* 30 (1987) 2372.
15. V. H. Schäfer, L. Bayer, Das Zustandsdiagramm Eisen (III)-chlorid-Eisen (II)-chlorid, *Z. anorg. Allg. Chem.* 271 (1953) 338 – 346.
16. N. G. Korzhukov, Y. B. Kabonin, Melting diagrams of the FeCl₂-CuCl₂ and CoCl₂-CuCl₂ systems. *Vestnik Moskovskogo Universiteta, Seriya 2: Khimiya*, 21 (1966) 66-68.
17. D. S. Coleman, P. D. A. Lacy, Phase equilibrium diagrams of the system calcium chloride-cuprous chloride-plumbous chloride. *Inst. Mining Met., Trans. Sect. C*, 77, (1968) C170-C173.
18. J.C. Zhao, J.F. Smith, Methods for Phase Diagram Determination, Introduction to phase diagrams, Elsevier Amsterdam, First Edition 1 (2007) 10 – 13
19. A.F. Holleman, E. Wiberg, Inorganic Chemistry, Academic Press San Diego (2001), ISBN: 0123526515.
20. A.F. Wells, Structural Inorganic Chemistry, Oxford: Clarendon press (1984) ISBN: 0198553706.
21. A.K. De, A Textbook of Inorganic Chemistry, 9th edition, New Age International (P) Ltd. Publishers, New Delhi (2003).
22. G. De Micco, D. M. Pasquevich, A. E. Bohé, Interactions during the chlorination of a copper–zinc alloy. *Thermochim. Acta*, 470 (2008) 83-90.
23. G. DeMicco, F.J. Alvarez, A.E. Bohe, D.M. Pasquevich, Chlorination applied to separation of metals, Sohn International Symposium Advanced Processing of Metals and Materials, New, Improved and existing technologies Iron and steel and recycling and waste treatment, TMS 5 (2006) 403 -418.
24. J.L. Pouchou and F. Pichoir, Advanced Quantitative Procedures for analytical SEM and EPMA: X-ray microanalysis of light elements and layered specimens, 10th European Congress on Electronic Microscopy (EUREM 92) (1992) 1 – 5.
25. M. Hillert, Phase Equilibria, Phase Diagrams and Phase Transformations, Their Thermodynamic Basis, Mathematical modelling of solution phases, Cambridge University Press, Cambridge (1998) 458 – 499.
26. H.S. Lukas, S.G. Fries, B. Sundman, Computational Thermodynamics, The Calphad Method, Models for the Gibbs energy, Cambridge University Press, New York, First edition (2007) 79 – 157.
27. D. Lindberg, Thermochemistry and melting properties of alkali salt mixtures in black liquor conversion processes, Doctoral Thesis, Åbo Akademi, Process Chemistry Centre, Laboratory of Inorganic Chemistry (2007) 9-26.

28. A.D. Pelton, S.A. Degterov, G. Eriksson, C. Robelin, Y. Dessureault, The modified Quasichemical model 1 – Binary Solutions, *Metall. Mater. Trans. B*, 31B, (2000) 651– 659.
29. A.D. Pelton, P. Chartrand, The modified Quasi-chemical model: Part II. Multicomponent Solutions, *Metall. Mater. Trans. A*, 32A (2001) 1355 – 1360.
30. P. Chartrand, A.D. Pelton, The Modified Quasi-chemical Model: Part III. Two sublattices, *Metall. Mater. Trans. A*, 32A (2001) 1397-1407.
31. A.D. Pelton, P. Chartrand, G. Eriksson, The Modified Quasi-chemical model: Part IV. Two-Sublattice Quadruplet Approximation, *Metall. Mater. Trans. A*, 32A (2001) 1409-1416.
32. C. Robelin, P. Chartrand, A.D. Pelton, Thermodynamic evaluation and optimization of the (MgCl₂ + CaCl₂ + MnCl₂ + FeCl₂ + CoCl₂ + NiCl₂) system, *J. Chem. Thermodynamics*, 36 (2004) 793 – 808.
33. C. Robelin, P. Chartrand, A.D. Pelton, Thermodynamic evaluation and optimization of the (NaCl + KCl + MgCl₂ + CaCl₂ + MnCl₂ + FeCl₂ + CoCl₂ + NiCl₂) system, *J. Chem. Thermodynamics*, 36 (2004) 809 – 828.
34. K.Wang, C. Robelin, Z. Wu, C. Li, L. Xie, P. Chartrand, Thermodynamic description of the AgCl-CoCl₂-InCl₃-NaCl system, *J. Alloys and Compounds*, 663 (2016) 885 – 898.
35. D.M. Ruthven, N.C. Kenney, Equilibrium Chlorine pressures over cupric chloride melts, *J. Inorg. Nucl. Chem*, 30 (1968) 931-944.
36. M. Hillert, The compound energy formalism, *J. Alloys and Compounds*, 320 (2001) 161-176.
37. T. Kekesi, K. Mimura, M. Isshiki, Copper Extraction from chloride solutions by evaporation and reduction with hydrogen, *Mater. Trans. JIM*, 36 (1995) 649 – 658.
38. F. Jones, H. Tran, D. Lindberg, L. Zhao, M. Hupa, Thermal Stability of Zinc Compounds, *Energy Fuels*, 27 (2013) 5663-5669.
39. D. Verhulst, A. Buekens, P.J. Spencer, G. Eriksson, Thermodynamic behavior of metal chlorides and sulfates under the conditions of incineration furnaces, *Environ. Sci. Technol*, 30 (1996) 50 – 56.
40. G.J. Janz, F.W. Dampier, G.R. Lakshminarayanan, P.K. Lorenz, R.P. Tomkins, Molten salts: Volume 1, Electrical conductance, Density and viscosity data, National standard reference data series, National Bureau of Standards 15 (1968) 42 – 108.
41. M. Gaune-Escard, Molten salts: from fundamentals to applications, NATO Science series, M.P. Tosi, Molten salts fundamentals (interionic forces and relevant statistical mechanics) Kluwer academic publishers, Kas Turkey, (2001) 1-4.
42. A.Romero-Serrano, A. Hernandez-Ramirez, A. Cruz-Ramirez, M. Hallen-Lopez, B. Zeifert, Optimization and calculation of the MCl-ZnCl₂ (M= Li, Na, K) phase diagrams, *Thermochim. Acta*, 510 (2010) 88–92.
43. R.Busch, The Thermophysical properties of Bulk metallic glass forming liquids, *JOM*, July (2000) 39 -42.
44. R.D. Shannon, Revised Effective Ionic radii and systematic studies of interatomic distances in halides and chalcogenides, *Acta Cryst. A* 32 (1976) 751 – 767.
45. S.N. Flengas, A.S. Kucharski, Theory of Enthalpy of Mixing, in Reactive Charge Asymmetrical Molten salt systems. Part 1. Binary Solutions, *Can. J. Chem.* 49 (1971) 3971-3985.
46. M.Asano, T.Sasaki, T. Abe, Y. Mizutani, T. Harada, Mass Spectrometric study of vaporization of FeCl₃-graphite intercalation compound, *J. Phys. Chem Solids*, 57, (1996) 787 – 790.
47. Z. Akdeniz, M.P. Tosi, The molten state of iron trichloride A molecular ionic conductor, *Il Nuovo cimento*, 20 D (1998) 1111 – 1115.

